

mmE-Loc: Facilitating Accurate Drone Landing with Ultra-High-Frequency Localization

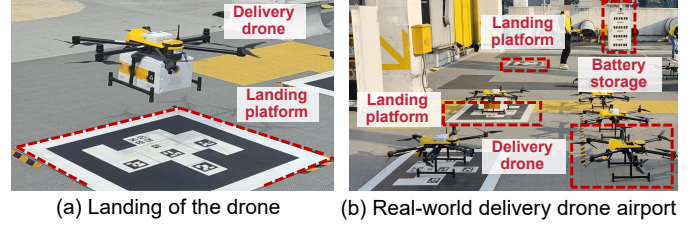
Haoyang Wang, Jingao Xu, Xinyu Luo, Ting Zhang, Xuecheng Chen, Ruiyang Duan, Jialong Chen, Yunhao Liu, *Fellow, IEEE*, Jianfeng Zheng, Weijie Hong, Xinlei Chen, *Member, IEEE*

Abstract—For precise, efficient, and safe drone landings, ground platforms should real-time, accurately locate descending drones and guide them to designated spots. While mmWave sensing combined with cameras improves localization accuracy, lower sampling frequency of traditional frame cameras compared to mmWave radar creates bottlenecks in system throughput. In this work, we upgrade traditional frame camera with event camera, a novel sensor that harmonizes in sampling frequency with mmWave radar within ground platform setup, and introduce mmE-Loc, a high-precision, low-latency ground localization system designed for precise drone landings. To fully exploit the *temporal consistency* and *spatial complementarity* between these two modalities, we propose two innovative modules: (i) the Consistency-instructed Collaborative Tracking module, which further leverages the drone’s physical knowledge of periodic micro-motions and structure for accurate measurements extraction, and (ii) the Graph-informed Adaptive Joint Optimization module, which integrates drone motion information for efficient sensor fusion and drone localization. Real-world experiments conducted in landing scenarios with a drone delivery company demonstrate that mmE-Loc significantly outperforms state-of-the-art methods in both accuracy and latency.

Index Terms—Drone ground localization; Event camera; mmWave radar

I. INTRODUCTION

Projected to soar to a \$1 trillion market by 2040 [2], the drone-driven low-altitude economy is transforming sectors with revolutionary applications such as on-demand delivery [3]–[6], meticulous industrial inspections [7]–[9], and rapid relief-and-rescue [10]–[14]. Of paramount importance within this burgeoning sector is the *landing phase*, where ground platforms locate drones descending from below 10 meters and guide them to accurately land at designated spots (Fig.1a) [15], [16]. Situated near populated and commercial zones, these operations emphasize safety and reliability: our research with a leading drone delivery company reveals that a landing bias of



Sensor type	2D imaging	Depth sensing	Output rate compatible with flight controller (Over 150Hz)
Frame camera	✓	✗	✗
mmWave radar	✗	✓	✓
mmWave radar + Frame camera	✓	✓	✗
Event camera	✓	✗	✓
mmWave radar + Event camera	✓	✓	✓

(c) Sensing capability of different sensor type

Fig. 1. Snapshot of drone landing phase, deliver drone airport, and performance of different sensors. (a) A delivery drone lands on the landing platform. (b) The real-world drone airport is equipped with multiple drones for package delivery. (c) Integrating mmWave radar with event camera combines reliable depth sensing and 2D imaging at ultra-high sampling frequencies. This solution achieves high spatio-temporal resolution 2D sensing and precise depth sensing for drone ground localization, while maintaining full compatibility with flight controllers by operating at update frequencies exceeding 150Hz.

just 10cm will result in drones missing charging ports, damaging delivery targets, or even posing risks to people [17]. Such inaccuracies undermine operational efficiency of this rapidly growing sector, potentially leading to severe consequences.

Widely adopted and straightforward approaches involve installing cameras at the center or edges of drone landing pads and employing computer vision algorithms for drone localization [18]–[20]. However, traditional frame cameras’ Achilles heel is capturing only 2D images without depth information, leading to scale uncertainty that limits the 3D localization accuracy [21]–[23]. To address this shortcoming, current practices have incorporated mmWave sensing to provide the lacked depth information for better localization accuracy and reliability in various conditions [24]–[30].

Albeit inspiring, our benchmark study with a world-leading drone delivery company in landing scenarios (Fig.1b) reveals another critical drawback (Fig.1c): the long exposure times of frame cameras ($> 20ms$) prevent their sampling rates from matching the high frequency of mmWave radars (e.g., 200Hz). This limitation creates system efficiency and throughput bottlenecks, restricting drone location updates to $< 50Hz$. In contrast, drone flight controllers typically require location input rates $> 150Hz$ to precisely adjust the drone’s flight attitude for safe landing [31], [32]. The inefficiency originates from the inherent physical limitations of conventional frame

A preliminary version of this work appeared in the 23rd ACM Conference on Embedded Networked Sensor Systems (ACM SenSys 2025) [1].

Haoyang Wang, Xinyu Luo, Xuecheng Chen, Ting Zhang and Xinlei Chen are with Shenzhen International Graduate School, Tsinghua University, China. (E-mail: {haoyang-22, luo-xy23, chenxc21}@mails.tsinghua.edu.cn, zhangt2112@gmail.com, chen.xinlei@sz.tsinghua.edu.cn).

Jingao Xu is with Carnegie Mellon University, USA. (E-mail: jingaox@andrew.cmu.edu)

Ruiyang Duan and Jialong Chen are with Meituan Academy of Robotics Shenzhen and Meituan Inc., China. (E-mail: {duanruiyang, chen-jialong02}@meituan.com)

Yunhao Liu is with the School of Software and BNRist, Tsinghua University, China. (E-mail: yunhao@greenorbs.com)

Jianfeng Zheng and Weijie Hong are with Shenzhen Smart City Communication Co., Ltd., China. (E-mail: {hongweijie, zhengjianfeng}@smartcitysz.com)

Corresponding author: Xinlei Chen.

Manuscript submitted: July 2025.

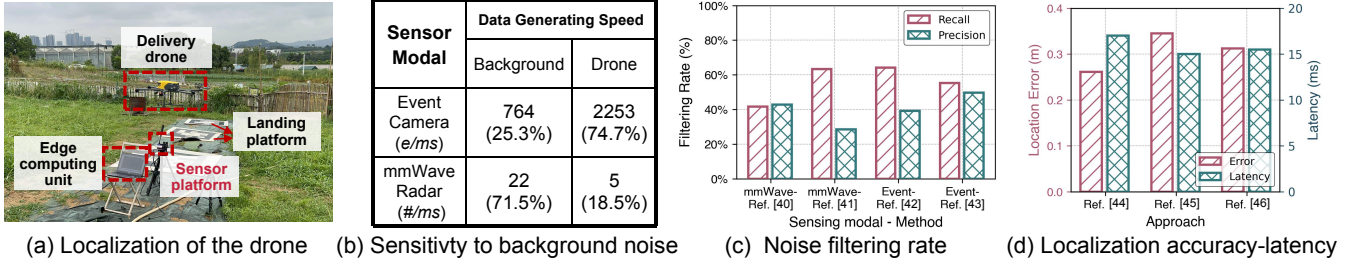


Fig. 2. Benchmark study on drone localization. (a) We conduct the benchmark study at a real-world drone delivery airport. (b) Both the event camera and mmWave radar are sensitive to environmental variations, leading to significant sensing noise. (c) Existing algorithms focus only on either mmWave radar or event cameras, failing to leverage the correlation between the two sensors, resulting in poor noise filtering performance. (d) These algorithms are prone to cumulative drift errors and experience considerable delays.

cameras and cannot be easily solved by software solutions.

Upgrade frame camera to event camera. Event cameras are bio-inspired sensors that report pixel-wise intensity changes with ms -level resolution [33]–[35], capturing high-speed motions without blurring [36], [37], ideal for fast-tracking tasks [38]. Event cameras offer ms -level sampling latency, which harmonizes exceptionally with the high sampling frequencies of mmWave radar. Their 2D imaging capability also complements radars' limited spatial resolution, similar to how traditional frame cameras operate. Such *temporal-consistency* and *spatial-complementarity* across event camera and mmWave radar inspire us to upgrade the frame camera with an event camera, pairing it with the mmWave radar to enable accurate and low-latency drone localization.

Our work. Following the above insight, we present **mmE-Loc**, the first active, high-precision, and low-latency landing drone ground localization system that enhances mmWave radar functionality with event cameras. mmE-Loc operates effectively in scenarios where the urban canyon effect degrades the accuracy of GPS or RTK systems, particularly as altitude decreases, rendering them nearly ineffective during the landing phase. With mmE-Loc, drones can achieve reliable localization in such scenarios, even under challenging conditions (e.g., low illumination), ensuring stable and efficient landings.

However, our benchmark study at a real-world drone delivery airport (Fig.2a) highlights several challenges that have been solved in making **mmE-Loc** a viable system outdoors:

(i) *How to accurately extract drone-related measurements* given the immense noisy output of event cameras and mmWave radars, which also lack inherent drone semantic information and differ greatly in dimension and pattern? Both modalities are sensitive to environmental variations, as shown in Fig.2b. Existing algorithms [39]–[42] are typically designed for single-modality, resulting in low noise filtering rates (recall and precision $< 65\%$ in Fig.2c).

(ii) *How to efficiently fuse event camera and mmWave measurements* that are heterogeneous in measurements precision, scale, and density? Existing EKF (extended Kalman filter) or PF (particle filter) based methods [43]–[45], suffer from the cumulative drift errors, making them insufficient for precise drone localization (Fig.2d).

(iii) *How to further optimize the efficiency of the fusion algorithm* to achieve high-frequency drone ground localization, given the limited computational resources on the landing platforms? Existing methods experience significant process-

ing delays, rendering them unsuitable for low-latency drone localization tasks (Fig.2d) [43]–[45].

To solve the above challenges, the design of mmE-Loc excel in the three aspects of drone ground localization:

- *On system architecture front.* Upgrading frame camera to event camera with ms -level latency to pair with the mmWave radar, mmE-Loc improves accuracy and efficiency of drone ground localization at data source level. The system architecture tightly integrates both modalities, from early-stage noise filtering and drone detection to later-stage fusion and optimization, fully leveraging advantages of both sensors (§II-A).
- *On system algorithm front.* We introduce a Consistency-instructed Collaborative Tracking (CCT) module, which leverages the drone's physical knowledge of periodic micro-motions and structure, along with cross-modal *temporal-consistency*, to filter environment-induced noise and achieve accurate drone detection (§III-A). We then present a Graph-informed Adaptive Joint Optimization (GAJO) module, which fuses *spatial-complementarity* with a novel factor graph to enhance accuracy of drone ground localization, while incorporating drone motion information as a constraint to improve efficiency, resulting in a trajectory with minimal bias and low cumulative drift (§III-B).
- *On system implementation front.* We further analyze the sources of latency and propose an incremental optimization method to further improve efficiency of the GAJO algorithm. This approach allows GAJO to dynamically optimize a set of locations, maintaining accuracy while reducing latency (§IV).

We fully implement mmE-Loc using a COTS event camera and mmWave radar. Over 30+ hours of indoor and outdoor experiments under various drone flight conditions assess its localization accuracy and end-to-end latency performance against four SOTA methods. mmE-Loc achieves an average localization accuracy of $0.083m$ and latency of $5.12ms$, surpassing baselines by $>48\%$ and $>62\%$, respectively, and showing minimal sensitivity to drone type and environment. We also deploy mmE-Loc at a real-world drone delivery airport (Fig.2a) for 10+ hours, demonstrating its practicality for commercial-level drone landing requirements.

In summary, this paper makes the following contributions.

- (1) We explore a novel sensor configuration, event camera plus mmWave radar, that harmonizes ultra-high sampling frequencies and propose mmE-Loc, a ground localization system for drone landings that delivers cm accuracy and ms latency.
- (2) We present CCT, which leverages *temporal consistency*

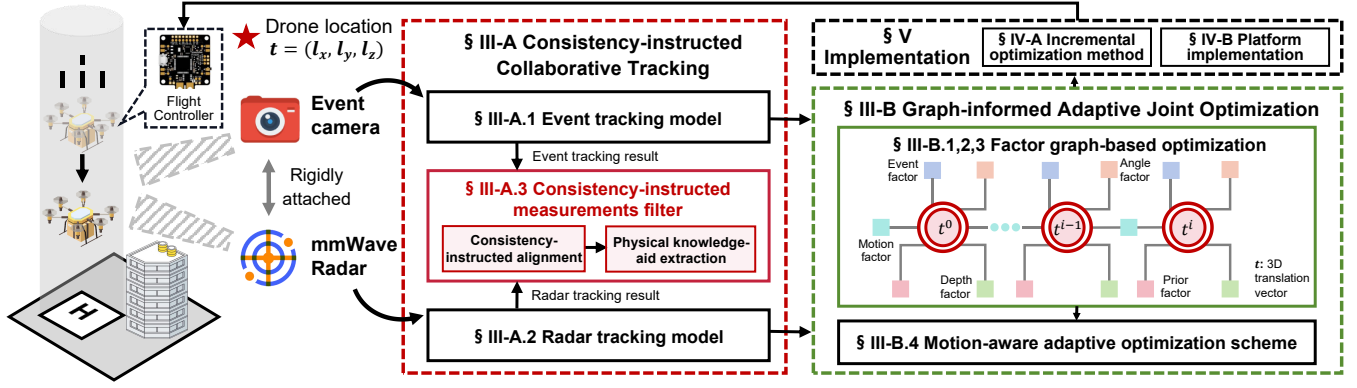


Fig. 3. System architecture of mmE-Loc. mmE-Loc consists of two main components. The first is Consistency-instructed Collaborative Tracking, which performs noise filtering on the data output by both the event camera and mmWave radar. It leverages the drone's physical knowledge of periodic micro-motions and structure for drone detection and provides a preliminary localization result for the drone. The second component is Graph-informed Adaptive Joint Optimization. This module designs various factors such as event factors and depth factors, and incorporates prior knowledge about the drone's motion through a prior factor. It adapts a factor graph for joint optimization to achieve trajectory optimization for drone. This module also introduces an adaptive window mechanism that dynamically adjusts the joint optimization window based on localization performance, reducing the number of parameters to be optimized. For implementation, mmE-Loc further introduces an Incremental Optimization Method to accelerate the solution process.

and the drone's physical knowledge of periodic micro-motions and structure for precise drone detection; and *GAJO*, which employs *spatial complementarity* with a novel factor graph, along with drone motion information to enhance localization. (3) We implement and extensively evaluate mmE-Loc by comparing it with four SOTA methods, showing its effectiveness. We also deploy mmE-Loc in a real-world drone delivery airport, demonstrating feasibility of mmE-Loc.

II. SYSTEM OVERVIEW

The mmE-Loc enhances the mmWave radar with an event camera to achieve accurate and low-latency drone ground localization, allowing the drone to rapidly adjust its location state and perform a precise landing. Given the critical importance of safety in commercial drone operations, mmE-Loc can work in conjunction with RTK or visual markers to ensure precise and robust landing performance. In this section, we mathematically introduce the problem that mmE-Loc tries to address and provide an overview of the system design.

A. Problem formulation

In this section, we illustrate key variables in mmE-Loc and introduce the system's inputs and outputs.

Reference systems. There are four reference (a.k.a., coordinate) systems in mmE-Loc: (i) the Event camera reference system E; (ii) the Radar reference system R; (iii) the Object reference system O; (iv) the Drone reference system D. Note that a drone can be considered as an object. For clarity, before an object is identified as a drone, we utilize O. Once confirmed as a drone, we use D for the drone and continue using O for other objects. Throughout the operation of system, E and R remain stationary and are rigidly attached together, while O and D undergo changes in accordance with movement of the object and the drone, respectively. The transformation from R to E can be readily obtained from calibration [46].

Goal of mmE-Loc. The goal of mmE-Loc is to determine 3D location of the drone, defined as t_{ED} , the translation from coordinate system D to E. Specifically, mmE-Loc optimizes and reports 3D location of drone (l_x, l_y, l_z) at each timestamp i with input from event stream and radar sample. t_{ED} and $(l_x,$

$l_y, l_z)$ are equivalent representations of the drone's location and can be inter-converted with Rodrigues' formula [47]. The former representation is adopted in the paper, as it is commonly used in drone flight control systems.

B. Overview

As illustrated in Fig.3, mmE-Loc comprises two key modules and task-oriented implementation:

- The *CCT* (Consistency-instructed Collaborative Tracking) for event camera and mmWave radar noise filtering, drone detection, and preliminary localization of the drone. This module utilizes time-synchronized event streams and mmWave radar measurements as inputs. The *radar tracking model* processes radar measurements to generate a sparse 3D point cloud. Meanwhile, the *event tracking model* takes into the stream of asynchronous events for event filtering, drone detection, and tracking. Finally, *consistency-instructed measurements filter* aligns the outputs of both tracking models by leveraging *temporal-consistency* between the two modalities. It then utilizes the drone's physical knowledge to extract drone-specific measurements and achieve drone preliminary localization. Specifically, this method exploits two key characteristics of the landing drone: (i) the high-frequency event bursts caused by the rapid micro-motions of the propellers, and (ii) the drone's symmetrical structure causes these events to exhibit axial symmetry, both of which serve as distinctive signatures for identifying the drone.

- The *GAJO* (Graph-informed Adaptive Joint Optimization) for fine and low-latency localization and trajectory optimization of the drone. Based on the operational principles of two sensors and their respective noise distributions, *GAJO* incorporates a meticulously designed *factor graph-based optimization* method. This module employs the *spatial-complementarity* from both modalities to unleash the potential of event camera and mmWave radar in drone ground localization. Specifically, *GAJO* jointly fuses the preliminary location estimation from the *event tracking model* and the *radar tracking model* and refines them. To reduce latency, we thoroughly analyze its underlying sources and introduce a motion-aware adaptive optimization scheme. By exploiting the drone's inherent motion

information, this method triggers optimization at appropriate times and adaptively adjusts the optimization window size, achieving precise localization with ms -level latency.

III. SYSTEM DESIGN

In this section, we introduce CCT for noise filtering, detection, and preliminary localization of drone (§ III-A). Subsequently, we delve into GAJO for fine and low-latency localization and trajectory optimization of drone (§ III-B).

A. CCT: Consistency-instructed Collaborative Tracking

The mmWave radar is prone to signal multipath effects, leading to inaccurate point cloud data. Meanwhile, the event camera captures per-pixel brightness changes asynchronously, which are frequently influenced by non-drone factors such as shadows. However, the absence of intrinsic drone semantic information, combined with significant differences in dimension and patterns between these two modalities, presents challenges for noise filtering. This results in drone detection bottlenecks, which further reduce the efficiency and accuracy of localization. Therefore, in this part, we focus on enhancing noise filtering and drone detection, while providing preliminary localization of the drone.

To address this challenge, we explore the operational principles of both sensors. Our design is based on observations: (i) *Event camera and mmWave radar demonstrate temporal consistency and distinct response mechanisms.* Event camera and mmWave radar maintain ms -level latency. Event cameras are unaffected by multipath effects, whereas mmWave radar remains impervious to changes in brightness. (ii) *Drone exhibits periodic micro-motion features (e.g., propeller rotation) and symmetrical structure,* which can serve as stable and distinctive features of drone. The high-speed periodic rotation of the drone's propellers causes rapid changes in light, leading to a large number of events. Moreover, due to the drone's symmetrical structure, these events also exhibit axial symmetry. These facilitate efficient cross-modal noise filtering by aligning measurements from the event camera and mmWave radar and enable drone detection by extracting drone measurements through periodic micro-motions.

To realize this idea, we design *CCT*, a lightweight cross-modal drone detector and tracker. *CCT* includes several components: (i) a radar tracking model (§III-A1) providing sparse point cloud indicating distance and direction information of objects; (ii) an event tracking model (§III-A2) for event filtering, detection, and tracking of objects; (iii) a consistency-instructed measurements filter (§III-A3) utilizes temporal consistency between both modalities and drone's periodic micro-motion features to extract event detection and point cloud of drone, facilitating the preliminary localization.

1) **Radar tracking model:** In this part, we calculate the distance D and direction vector \vec{v} between the radar and objects, along with a preliminary estimation of the object's location, as depicted in Fig.4 and Fig.5.

Distance calculation. As shown in Fig.4, the frequency difference between the transmitted (TX) and received (RX)

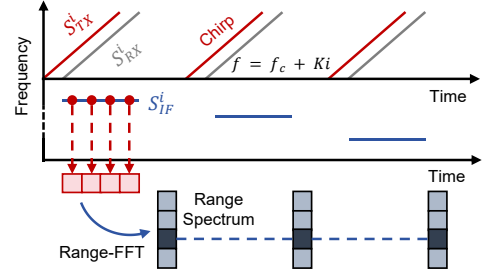


Fig. 4. Distance calculation by frequency difference

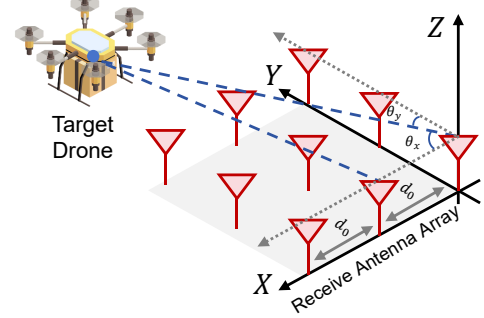


Fig. 5. Direction calculation by phase difference

signals indicates the signal propagation time, revealing distance between object and radar. Denoting D^i as the distance at time i , TX and RX signals as:

$$S_{TX}^i = \exp[j(2\pi f_c i + \pi K i^2)], S_{RX}^i = \alpha S_{TX}^i \left[i - \frac{2D^i}{c} \right], \quad (1)$$

where α denotes the attenuation rate, f_c is the initial frequency, K represents the chirp slope of FMCW signal, and c stands for light speed. The TX and RX signals undergo mixing and low-pass filter (LPF) to extract intermediate frequency signal (IF signal) $s(t)$:

$$S_{IF}^i = LPF(S_{TX}^{i*} S_{RX}^i) \approx \alpha \exp \left[j2\pi \left(\frac{2KD^i}{c} \right) i \right]. \quad (2)$$

The frequency value f_{IF} within S_{IF}^i encapsulates distance information. After the Range-FFT operation of S_{IF}^i , f_{IF} is extracted, facilitating distance calculation $D^i = \frac{c f_{IF}}{2K}$.

Direction calculation. Using a fixed antenna array, the mmWave radar determines the object's direction by employing two orthogonal linear arrays. As depicted in Fig.5, each linear array captures an Angle of Arrival (AoA), calculated from the phase difference between adjacent antennas spaced apart by d as $\cos\theta = \Delta\phi\lambda/2\pi d$, where θ represents AoA, λ denotes the wavelength and $\Delta\phi$ indicates the phase difference. With two orthogonal arrays, the radar obtains two AoAs, θ_x and θ_y . The unit vector indicating object's direction \vec{i} is given by

$$\vec{v}^i = [\cos\theta_x \cos\theta_y \sqrt{1 - \cos^2\theta_x - \cos^2\theta_y}]^T. \quad (3)$$

Using the distance and angle information obtained above, along with the spatial relationship between radar and event camera, we can determine the preliminary 3D location estimation of object in E as $P_E = D\vec{v} + t_{ER}$. We then leverage

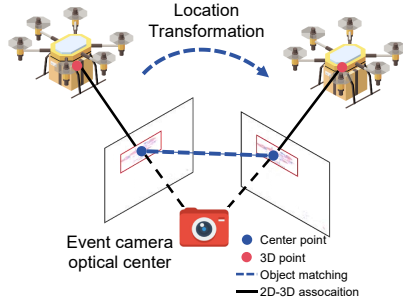


Fig. 6. Event tracking model

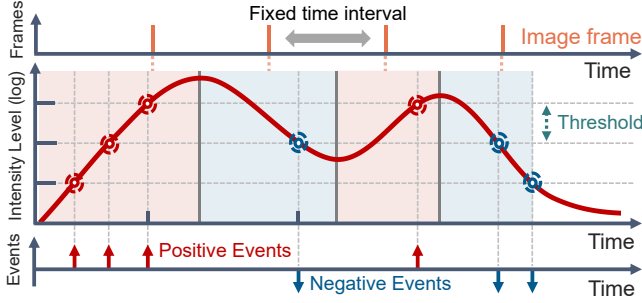


Fig. 7. Illustration of synchronous frames from frame camera and asynchronous events from event camera. Frame cameras capture images at fixed intervals using a global shutter. In contrast, event cameras operate asynchronously. Each pixel in an event camera responds independently, generating events whenever intensity changes exceed a threshold.

the mmWave radar for object 3D location tracking, estimating the translation t_{EO} of object at time i :

$$\begin{aligned} t_{EO}^i &= t_{EO}^{i-1} + U_E^i + w^i + w^{i-1} \\ &= t_{EO}^{i-1} + (P_E^i - P_E^{i-1}) + w^i + w^{i-1}. \end{aligned} \quad (4)$$

U_E^i is discrepancy between two radar results at times i and $i-1$ in E . w_i and w_{i-1} signify measurement noise.

While mmWave radars are effective in estimating object depth along the radial direction, they exhibit limited accuracy in capturing motion along the horizontal and vertical (tangential) directions [48], [49]. To overcome this limitation, we incorporate an event camera, which, despite having comparable latency, operates based on a fundamentally different sensing principle. Thanks to its high spatial resolution, the event camera enhances object detection and effectively complements the mmWave radar by providing accurate motion information in the tangential plane.

2) Event tracking model: In this part, we demonstrate the process of noise filtering from a stream of asynchronous events, and how to detect and track objects with the filtered events, as depicted in Fig.6. As illustrated in Fig.7, unlike conventional frame-based cameras that rely on a global shutter to capture images at fixed intervals, event cameras asynchronously record per-pixel intensity changes with ms -level temporal resolution and latency. This enables high-speed motion capture without motion blur, but also introduces challenges in noise suppression and object detection.

Similarity-informed event filtering. Event cameras are prone to noise from transistor circuits and other non-idealities, requiring pre-processing filtering. For the i^{th} event $e_{(x,y)}^i$ with the timestamp $t_{(x,y)}^i$, we assess the timestamp ($t_{n(x,y)}^i$) of the most recent neighboring event in all directions. Events with a time difference less than the threshold T_n are retained, indicat-

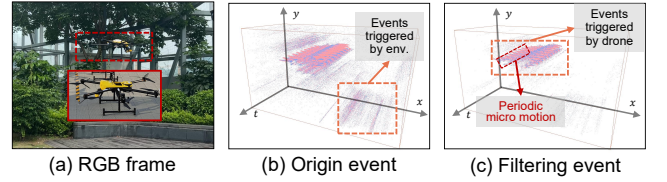


Fig. 8. Event filtering performance. mmE-Loc leverages neighborhood similarity for event noise filtering and uses the Surface of Active Events to manage events. This approach ensures precise spatio-temporal representation, reduces the number of events, and conserves computational resources.

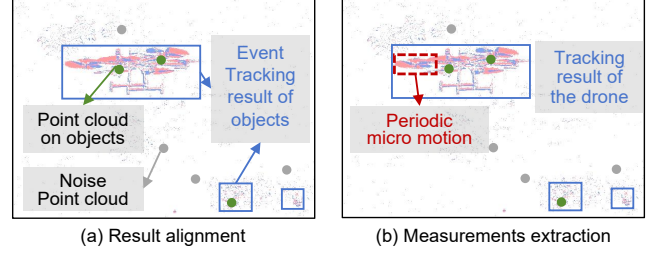


Fig. 9. Consistency-instructed Measurements Filter. (a) The event camera and mmWave radar are rigidly attached, so their spatial relationship is known in advance. By leveraging their temporal consistency, we can align the outputs of the two sensors in the spatio-temporal domain, enabling the detection of the drone and other objects. (b) The drone's propellers operate at high frequencies, causing rapid changes in light intensity and generating a large number of events. Additionally, the drone's symmetrical structure causes these events to exhibit axial symmetry, which serves as a key feature for distinguishing the drone from other objects.

ing object activity, while those exceeding it are discarded as noise (Fig.8b, Fig.8c). We utilize the Surface of Active Events (SAE) [50] to manage events, mapping coordinates (x, y) to timestamps (t_l, t_r) . Upon a new event's arrival, t_l updates accordingly, and t_r updates only if the previous event at the same location occurred outside the time window T_k or had a different polarity. Events that update value of t_r are retained. The event stream, segregated by polarity, is processed with distinct SAEs. This method ensures precise spatial-temporal representation, conserving computational resources.

Filter-based detection and tracking. We employ a grid-based method to cluster events to facilitate object detection. The camera's field of view is partitioned into elementary cells sized $c_w \times c_h$. For each cell, we compare the event count within a specified time interval ($c_{\Delta t}$) to an activation threshold c_{thres} . Cells surpassing c_{thres} are marked as active and connected to form clusters, serving as object detection results, including those generated by the drone. For tracking, we deploy Kalman filter-based trackers with a constant velocity motion model, which provides low-latency estimates with minimal computational cost [51]. A tracker predicts the state of the current object and associates it with the input cluster that has the largest IoU (Intersection over Union) area. The input cluster corrects tracker state, generating bounding boxes, and effectively tracking moving objects, including the drone.

Using bounding box proposals and pinhole camera model with projection function π , we estimate preliminary 3D locations of objects. Specifically, π transforms a 3D point \mathbf{X}_E into a 2D pixel x in image plane as:

$$\begin{aligned} x &= \pi(\mathbf{X}_E) = [f_x \frac{X_E}{Z_E} + c_x, f_y \frac{Y_E}{Z_E} + c_y]^T, \\ \mathbf{X}_E &= [X_E, Y_E, Z_E]^T, \end{aligned} \quad (5)$$

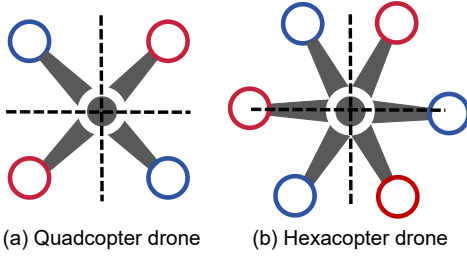


Fig. 10. The structure of both the quadcopter and hexacopter drones, which feature propellers arranged in axial symmetry.

where $[f_x, f_y]^T$ is focal length of the event camera, and $[c_x, c_y]^T$ denotes the principal point, both being intrinsic camera parameters. Then, the object's preliminary location at i is estimated using the center point of bounding box proposal x^i as:

$$x^i = \pi(\mathbf{X}_E^i) + v^i = \pi(\mathbf{X}_0^i + t_{EO}^i) + v^i, \quad (6)$$

where \mathbf{X}_0^i represents the corresponding 3D point of center point x^i in the object reference 0, v^i denotes the random noise. When extracting center points from bounding box proposals, we first undistort their coordinates.

3) Consistency-instructed measurements filter: The *event tracking model* detects drones and other objects causing light changes, such as indicator lights or shadows. The system must effectively differentiate events triggered by the landing drone from those induced by surrounding objects. Similarly, the radar tracking model generates a 3D point cloud comprising both valid drone reflections and spurious points resulting from multipath effects, requiring extraction of drone-related points.

Consistency-instructed alignment. Utilizing the *temporal-consistency* from the event camera and mmWave radar, and their distinct mechanisms respond to dynamic objects, we can filter event camera results affected by lighting variations on stationary objects and vice versa for radar points influenced by multipath effects. Specifically, we align temporal-synchronized radar points (*radar tracking model*) to event bounding boxes (*event tracking model*) using spatial relationships of event camera and mmWave radar (Fig.9a). Using event camera's projection function, we determine that object's location lies along the ray from the camera's optical center through the bounding box center. The system then identifies the nearest radar points along this ray to isolate the object-associated points. If no radar point is detected, this bounding box is treated as noise and disregarded.

Drone physical knowledge-aid extraction. Since each platform supports one drone landing at a time, we need to identify distinguishing features of the landing drone, which effectively differentiates the drone from noise, and use it to extract landing drone-specific measurements from the aligned tracking results. Our findings reveal that drones exhibit periodic micro-motions (e.g., propeller rotation), and the events generated by these micro-motions display distinct structure characteristics (e.g., circular patterns). Due to the drone's symmetrical design, the periodic micro-motions of multiple propellers create events with notable symmetrical features (e.g., axial symmetry), which can serve as stable and distinctive features for the landing drone. Specifically, the rotation of the drone's propellers generates high-frequency motion patterns. Thanks

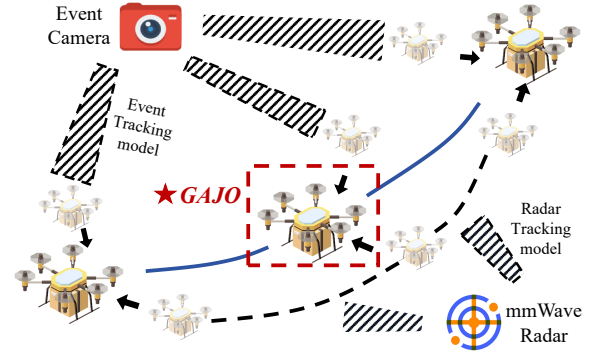


Fig. 11. Illustration of relationship between GAJO, event tracking model and radar tracking model. The GAJO module harnesses *spatial-complementarity* of both modalities through a factor graph-based join optimization, where event camera provides 2D imaging and mmWave radar delivers depth information.

to the high-frequency sensing capabilities of both sensors, these patterns can be effectively leveraged as distinguishing features, enabling the suppression of low-frequency noise commonly present in real-world environments. In extracting drone-related measurements, we leverage both the periodic micro-motion and shape features of propeller rotation, as well as the symmetry across different propellers.

(i) *Periodic micro motion feature-based extraction.* The rapid periodic micro-motions of the propellers induce high-frequency bursts of events, resulting in a significantly higher number of events generated by the drone compared to other objects in the environment. Therefore, we transform the spatio-temporal distribution of events into a heatmap and apply statistical metrics to isolate drone measurements leveraging this feature. Specifically, within a time window $[i, i + \delta i]$, events are binned into a 2D histogram where each bin corresponds to a spatial region (e.g., 5×5 pixels). Bins containing propeller rotation tend to accumulate more events due to rapid light intensity changes. Meanwhile, these propeller rotations generate bipolar events within a bin, while background motion and noise typically result in unipolar events (e.g., from flying birds). Therefore, we select bins with propeller rotation based on event counts and the proportion of positive events, favoring those with higher counts and a more balanced ratio.

(ii) *Structure-based extraction.* When other obstacles in environment undergo rapid motion, they may also generate a large number of events. Meanwhile, in such cases, the ratio of positive to negative events tends to be relatively balanced. To further filter out irrelevant measurements under these circumstances, we exploit the structure and symmetry characteristics of drone's propeller rotation. Specifically, for selected bins, we analyze their connectivity to form clusters and fit ellipses to the structure of the resulting bin clusters. Given that the delivery drone has four or six propellers arranged in axial symmetry as shown in Fig.10, we assess the symmetry of the ellipse-fitted bin clusters to determine whether the bounding box is generated by the drone. If the ellipse-fitted bin clusters exhibit axial symmetry, the bounding box is considered to be generated by the drone.

Finally, we identify event tracking results with the most bins indicative of propeller rotation and corresponding point clouds (t_{EO}), designating them as drone tracking results (t_{ED}) for preliminary localization from two models as shown in Fig.9b.

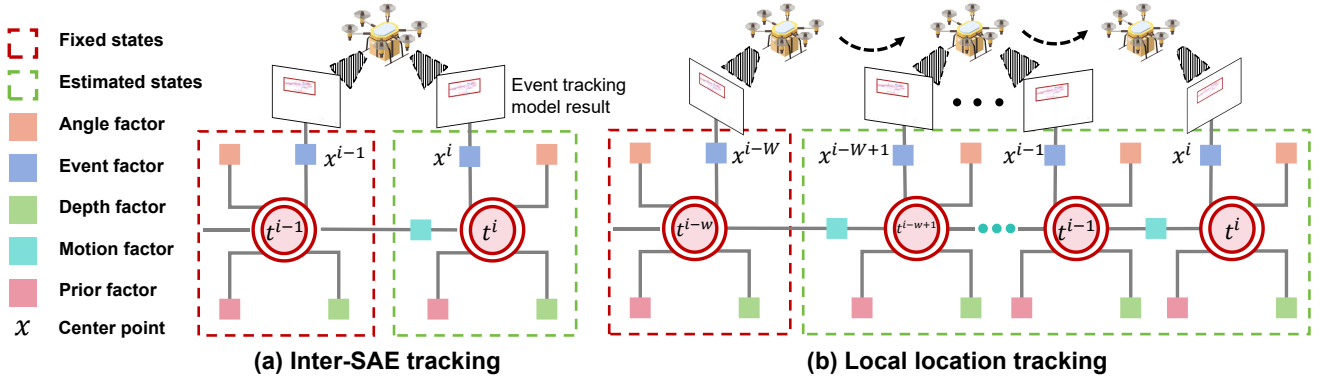


Fig. 12. Illustration of Graph-informed Adaptive Joint Optimization. The module consists of two parts. The first part is (a) Inter-SAE Tracking, which aims to perform short-term joint optimization for low-latency output. However, the localization results from this part may accumulate errors over time. Therefore, the second part, (b) Local Location Optimization, performs long-term joint optimization by jointly considering multiple locations and associated constraints, resulting in a trajectory with reduced bias and minimized cumulative drift.

When multiple drones are scheduled to land, they descend and land sequentially. This method accurately identifies the landing drone and extracts relevant measurements.

B. GAJO: Graph-informed Adaptive Joint Optimization

The preliminary drone location estimations from the event and radar tracking models suffer from biases. Specifically, estimations from event tracking model face scale uncertainty, while estimations from radar tracking model struggle with limited spatial resolution, scatter center drift, and accumulating drift. Additionally, estimations from different models are heterogeneous in precision, scale, and density, complicating the fusion and optimization. Therefore, in this part, we prioritize accurate drone ground localization and trajectory tracking.

Our design is founded on the insight that *the event tracking model and radar tracking model provide distinct features that are spatial-complementarity to each other*. As a result, the 2D imaging capability of event camera and the depth sensing capability of mmWave radar mutually enhance each other when combined, as demonstrated in Fig.11. Since both the event stream and mmWave samples are drone-related, fully leveraging the *spatial-complementarity* of these two modalities through joint optimization offers the potential to significantly improve performance. This leads to a trajectory with reduced bias and minimized cumulative drift.

To realize this idea to push the limit of localization accuracy while minimizing latency, we introduce a *GAJO*, a factor graph-based location optimization framework designed for low-latency and accurate drone 3D localization (§III-B1). *GAJO* includes two parallel tightly coupled modules: (i) short-term tracking (inter-SAE tracking) and (ii) long-term optimization (local location optimization), collectively enhancing location tracking precision (§III-B3). Beyond the capabilities of *event tracking model* and *radar tracking model*, *GAJO* assimilates prior knowledge of drone's flight dynamics to refine the trajectory for enhanced smoothness and accuracy (§III-B2). To reduce the computational time of the optimization process, we leverage the drone's motion information to assess the quality of current localization. On one hand, this assessment helps determine whether long-term optimization is necessary; on the other hand, it enables adaptive adjustment of the optimization window size, thereby minimizing the computational overhead introduced by optimization.

1) Factor graph-based optimization: A factor graph comprises variable nodes, indicating the states to be optimized (e.g., t_{ED}^i), and factor nodes, representing the probability of certain states given a measurement result. In mmE-Loc, measurements are derived from the Event Tracking (ET) model (x^i) and Radar Tracking (RT) model (D^i , \bar{v}^i , and U_E^i). To estimate the values of a set of variable nodes $\mathcal{X} = \{t_{ED}^i | i \in \mathcal{T}\}$ given measurements $\mathcal{Z} = \{x^i, D^i, \bar{v}^i, U_E^i | i \in \mathcal{T}\}$, *GAJO* optimizes all connected factor nodes based on maximum a posteriori estimation:

$$\begin{aligned} \hat{\mathcal{X}} &= \arg \max_{\mathcal{X}} p(\mathcal{X} | \mathcal{Z}) = \arg \max_{\mathcal{X}} p(\mathcal{X}) p(\mathcal{Z} | \mathcal{X}) \\ &= \arg \max_{\mathcal{X}} p(\mathcal{X}) \prod_{i \in \mathcal{T}} p(x^i | t_{ED}^i) p(D^i, \bar{v}^i, U_E^i | t_{ED}^i), \end{aligned} \quad (7)$$

which follows the Bayes theorem. $p(\mathcal{X})$ is the prior information over $\mathcal{X} = \{t_{ED}^i | i \in \mathcal{T}\}$, which is inferred from drone flight characteristics. The $p(x^i | t_{ED}^i)$ is the likelihood of the ET model measurements. The $p(D^i | t_{ED}^i)$, $p(\bar{v}^i | t_{ED}^i)$ and $p(U_E^i | t_{ED}^i)$ are likelihood of the RT model measurements.

2) Probabilistic representation: Inferring the drone's location requires prior term and likelihood term in Eqn.(7).

Prior term. The prior term, $p(t_{ED}^i)$, represents the drone's location probability distribution at time i unaffected by current measurements. Derived from a constant velocity model, it suggests the drone maintains steady speed over short intervals, allowing us to predict the prior location using:

$$\bar{t}_{ED}^i - t_{ED}^{i-1} = t_{ED}^{i-1} - t_{ED}^{i-2}. \quad (8)$$

ET model likelihood. The likelihood $p(x^i | t_{ED}^i)$ from ET model represents the center point distribution at a given drone location. In many tracking systems [52], center point noise v^i is assumed Gaussian, proving effective. Thus, likelihood of ET model is:

$$p(x^i | t_{ED}^i) \sim \mathcal{N}(\pi(\mathbf{X}_E^i), \sigma_{ET}), \quad (9)$$

where σ_{ET} is the center point standard deviation.

RT model likelihood. The likelihood of the RT model $p(D^i | t_{ED}^i)$, $p(\bar{v}^i | t_{ED}^i)$ and $p(U_E^i | t_{ED}^i)$ indicates the distribution of the measured distance, angle, and motion at a

given drone location. The distance, angle, and motion from RT model likelihood are:

$$\begin{aligned} p(D^i | t_{ED}^i) &\sim \mathcal{N}(\|t_{ED}^i\|, \sigma_D), \quad p(\vec{v}^i | t_{ED}^i) \sim \mathcal{N}(\vec{v}_{t_{ED}^i}, \sigma_{\vec{v}}), \\ p(U_E^i | t_{ED}^i) &\sim \mathcal{N}(t_{ED}^i - t_{ED}^{i-1}, \sigma_{U_E}), \end{aligned} \quad (10)$$

where σ_D , $\sigma_{\vec{v}}$ and σ_{U_E} are the standard deviation of distance, angle, and motion measurements respectively.

3) **Fusion-based tracking:** In mmE-Loc, two fusion schemes are employed for sensor fusion and optimization, as depicted in Fig.12. The first, inter-SAE tracking, aims for instant drone location estimation by minimizing errors across different tracking models simultaneously. The second, local location optimization, enhances overall trajectory accuracy through the joint optimization of a selected set of locations.

Inter-SAE tracking. Once the measurements of ET model and RT model ($x^i, D^i, \vec{v}^i, U_E^i$) received, the prior factor, ET factor and the RT factor are formulated as follows:

$$\begin{aligned} E_{\text{Prior}}^i &= -\log p(t_{ED}^i) \propto \|t_{ED}^i - \bar{t}_{ED}^i\|_{\sigma_{t_{ED}}}^2, \\ E_{\text{ET}}^i &= -\log p(x^i | t_{ED}^i) \propto \rho(\|x^i - \pi(\mathbf{X}_E^i)\|_{\Sigma_E}^2), \\ E_{\text{RT}}^i &= -\log p(D^i, \vec{v}^i, U_E^i | t_{ED}^i) \\ &\propto \|\|t_{ED}^i\| - D^i\|_{\sigma_D}^2 + \|\vec{v}_{t_{ED}^i} - \vec{v}^i\|_{\sigma_{\vec{v}}}^2 + \\ &\quad \|(t_{ED}^i - t_{ED}^{i-1}) - U_E^i\|_{\sigma_{U_E}}^2, \end{aligned} \quad (11)$$

where $\|e\|_{\Sigma_E}^2 = e^T \Sigma^{-1} e$. The symbol Σ_E represents covariance matrix associated with event camera measurements.

On this basis, the inter-SAE tracking in Fig.12a is performed to give an instant location result based on Eqn.(7) as follows:

$$\begin{aligned} \hat{t}_{ED}^i &= \arg \max_{t_{ED}^i} p(t_{ED}^i | t_{ED}^{i-1}, t_{ED}^{i-2}) p(x^i | t_{ED}^i) p(D^i, \vec{v}^i, U_E^i | t_{ED}^i) \\ &= \arg \min_{t_{ED}^i} -\log(p(t_{ED}^i | t_{ED}^{i-1}, t_{ED}^{i-2}) p(x^i | t_{ED}^i) p(D^i, \vec{v}^i, U_E^i | t_{ED}^i)) \\ &= \arg \min_{t_{ED}^i} (E_{\text{prior}}^i + E_{\text{ET}}^i + E_{\text{RT}}^i). \end{aligned} \quad (12)$$

Local location optimization. To mitigate cumulative drift, local location optimization is conducted, correcting estimated locations based on multiple consecutive SAEs. This optimization entails jointly optimizing the locations of a SAE set denoted as $\mathcal{X} = \bigcup_{i \in \mathcal{T}} \{t_{ED}^i\}$, as shown in Fig.12b, where $W = |\mathcal{T}|$. The optimization problem formulation is as follows:

$$\begin{aligned} \hat{\mathcal{X}} &= \arg \max_{\mathcal{X}} p(\mathcal{X}) \prod_{i \in \mathcal{T}} p(x^i | t_{ED}^i) p(D^i, \vec{v}^i, U_E^i | t_{ED}^i), \\ &= \arg \min_{\mathcal{X}} \sum_{i \in \mathcal{T}} (E_{\text{prior}}^i + E_{\text{ET}}^i + E_{\text{RT}}^i). \end{aligned} \quad (13)$$

It is worth noting that (i) when the local location optimization is triggered, (ii) what is the size of \mathcal{T} ($W = |\mathcal{T}|$), and (iii) how to solve the inter-SAE tracking and local location optimization problems affect latency and accuracy of localization. Hence, we improve efficiency of GAJO through a motion-aware adaptive optimization scheme to address (i) and (ii), and an incremental optimization method in to solve (iii).

4) **Motion-aware adaptive optimization scheme:** In this section, we address two key issues: determining (i) when local location optimization should be triggered, and (ii) the size of \mathcal{T} . To solve these problems, we incorporate the drone's motion information. Specifically, a common sensor used in the drone's flight controller is the Inertial Measurement Unit (IMU), which outputs the drone's acceleration. By integrating this acceleration, we can calculate the drone's displacement between two timestamp. Using this motion information, we combine the location estimates from the optimization algorithm at time $i - j$ ($j \in \{1, \dots, W\}$) to predict the drone's location at time i . If the predicted location at i deviates from the optimization algorithm's output at i by more than a threshold Δ , we trigger the local location optimization for location set $\mathcal{X} = \bigcup_{k \in [i-j, i]} \{t_{ED}^k\}$.

Algorithm 1: Incremental optimization method.

Data: Original factor graph G ; New measurements D^i, \vec{v}^i, U_E^i ; square root information matrix R

Result: Updated locations $\hat{\mathcal{X}}$

```

1  $G \leftarrow \text{AddFactorToGraph}(G^i, D^i, \vec{v}, U_E^i)$ ;
2  $R \leftarrow \text{IncrementalUpdate}(G)$ ;
3  $\hat{\mathcal{X}} \leftarrow \text{Backsubstitution}(R)$ ;
4  $L \leftarrow \emptyset$ ;  $\triangleright$  Set of nodes need to be linearized;
5 for all  $t_{ED}^i \in \mathcal{X}$  and all  $\hat{t}_{ED}^i \in \hat{\mathcal{X}}$  do
6   if  $\hat{t}_{ED}^i - t_{ED}^i \geq \delta$  then
7      $L \leftarrow L \cup t_{ED}^i$ ;
8   end
9 end
10 if  $|L| \geq L_T$  or  $\|\hat{\mathcal{X}} - \mathcal{X}\| \geq \Delta$  then
11   for all  $t_{ED}^i \in \mathcal{X}$  do
12      $\text{UpdateLinearizationPoint}(t_{ED}^i)$ ;
13   end
14    $R \leftarrow \text{FullUpdate}(G)$ ;
15    $\hat{\mathcal{X}} \leftarrow \text{Backsubstitution}(R)$ ;
16 end
```

IV. IMPLEMENTATION

A. Incremental optimization method

Factor graph solving. We represent the estimation problems Eqn.(12) and Eqn.(13) using a factor graph model. To solve the nonlinear least-squares problems, we linearize the observation model and solve the least-squares formulation:

$$\hat{\mathcal{X}} = \arg \min_{\mathcal{X}} \|A\mathcal{X} - \mathbf{b}\|^2, \quad (14)$$

where $A \in \mathbb{R}^{m \times n}$ is the measurement Jacobian and $\mathbf{b} \in \mathbb{R}^m$ is the right-hand side vector. We then utilize QR matrix factorization [53] as $A = Q[R, 0]^T$ and solve the least squares problem $R\hat{\mathcal{X}} = \mathbf{d}$ through backsubstitution to obtain optimized locations $\hat{\mathcal{X}}$, where $R \in \mathbb{R}^{n \times n}$ is the upper triangular square root information matrix, $Q \in \mathbb{R}^{m \times m}$ is an orthogonal matrix, and $\mathbf{d} \in \mathbb{R}^n$ [54]. Although re-linearizing and regenerating R with new measurements can help mitigate errors, applying this approach to problem (13) can be computationally expensive, as

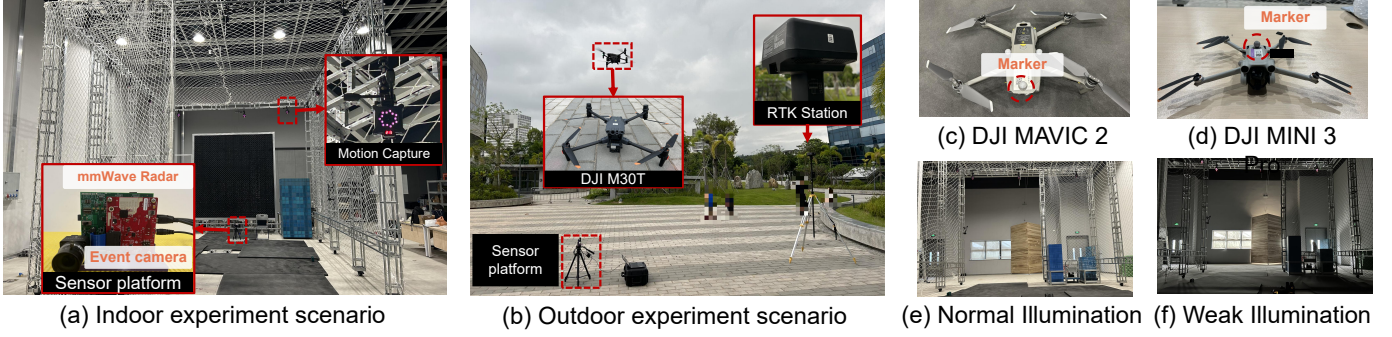


Fig. 13. Experimental setup and scenarios of mmE-Loc. (a) A laboratory scenario with motion capture system for ground-truth collection. (b) An outdoor scenario with RTK system for ground-truth collection. (c)-(d) Different drone with different size (DJI MAVIC 2 and DJI MINI 3 Pro). (e)-(f) Different illumination situation of the laboratory (normal and weak).

it requires frequent updates and increased processing overhead, limiting real-time performance.

Incremental optimization method. To tackle this, we propose an incremental optimization method, leveraging the insight that *new measurements mainly impact localized areas, leaving distant parts unchanged*. This allows us to incrementally update R during local optimization [55]. By adaptively combining updated and regenerated R , this method reduces latency and enhances accuracy.

Algorithm 1 shows how incremental optimization method solves local location optimization problem. Lines 1-3 depict tracking with incrementally updated R , while lines 4-16 show tracking with re-generated R . Specifically, when receiving new measurements, function `AddFactorToGraph` updates factor graph, and function `IncrementalUpdate` incrementally updates R with new measurements [55]. We then solve local location tracking with this incrementally updated R .

When one of two conditions is met, we solve local location tracking with re-generated R : (i) we track locations that have changed significantly in a set $L = \{t_{ED}^i : t_{ED}^i - t_{ED}^{i-1} \geq \delta\}$. If enough locations have undergone significant changes (i.e., $|L| \geq L_T$), we solve location tracking with re-generated R output by function `FullUpdate`. (ii) The norm of total location changes exceeds a threshold Δ (i.e., $\|\hat{\mathcal{X}} - \mathcal{X}\| \geq \Delta$). Since the local location tracking involves repeatedly solving linear equations, this condition keeps current solution from diverging too far from optimal solution.

B. Platform implementation

In this section, we will detail the platform implementation.

Sensor platform configuration. As illustrated in Fig.13, we implement our sensing platform with multiple sensors including (i) A Prophesee EVK4 HD evaluation kit, featuring the IMX636ES event-based vision sensor for HD event data (1280×720 pixels) with 47.0° FoV. (ii) A Texas Instruments (TI) IWR1843 board for transmitting and receiving mmWave signals within the frequency range of 76 GHz to 81 GHz with three transmitting antennas and four receiving antennas. These antennas are arranged in two linear configurations on the horizontal plane. (iii) An Intel D435i Depth camera for RGB image capture used in the baseline method.

Deployment detail. During the experiments, the sensor platform is placed at the center of the landing pad. In the real-world case study conducted at an airport, the platform

is positioned at the edge of the pad for safety reasons, with the distance from the platform to the pad's center being less than 1 meter. Once the drone takes off, it enters the event camera's field of view (FoV). All sensors are synchronized via the Robot Operating System (ROS). mmE-Loc runs on a PC with Ubuntu 20.04, equipped with an Intel i7-12900K CPU, 32GB of RAM, and an NVIDIA GeForce GTX 1070 GPU. For practical deployments, the sensor platform is ideally positioned at the center of the landing pad, with its height aligned to the pad's, ensuring that the drone remains within the event camera's FoV at all times for continuous localization.

V. EVALUATION

Our evaluation of mmE-Loc is comprehensive and grounded entirely in real-world experimentation. We begin with experimental settings in §V-A. Then, in §V-B, we focus on key performance metrics: localization accuracy and latency. §V-C delves into external factors impacting mmE-Loc, such as drone characteristics and environmental conditions. §V-D assesses benefits of sensor fusion and the performance of various modules. Finally, in §V-E, we evaluate system load, including latency, CPU usage, and memory consumption.

A. Experimental methodology

Experiment setting. We use a deployment setup and drone equipment that closely mimic real-world applications. Fig.13 shows the experimental scenarios in both an *indoor* laboratory and an *outdoor* flight test site. The setup in Fig.13a includes the event camera and mmWave radar mounted together *at the ground of the experimental area*. We evaluate mmE-Loc on various target drones: (i) *DJI Mini 3 Pro*: $0.25\text{m} \times 0.36\text{m} \times 0.07\text{m}$ with unfolded propellers. (ii) *DJI MAVIC 2*: $0.32\text{m} \times 0.24\text{m} \times 0.08\text{m}$ with unfolded propellers. (iii) *DJI M30T*: $0.49\text{m} \times 0.61\text{m} \times 0.22\text{m}$ with unfolded propellers. We conducted extensive experiments over 30 hours, collecting more than 400GB of raw data.

Ground truth. In the indoor scenario, we used a motion capture system with fourteen cameras. This system covers an $8\text{m} \times 8\text{m} \times 8\text{m}$ area, providing localization accuracy within 1 mm , allowing precise performance evaluation under controlled conditions. In the outdoor scenario, we conducted experiments at a secluded site with excellent GPS signal reception. We set up a Real-Time Kinematic Positioning (RTK) base station to rebroadcast the GPS signal phase, ensuring high-fidelity RTK

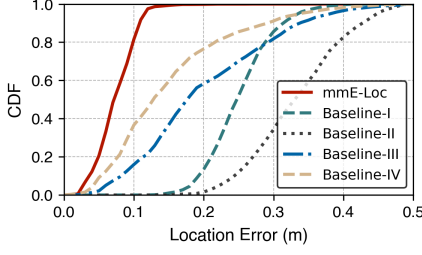


Fig. 14. Indoor accuracy comparison

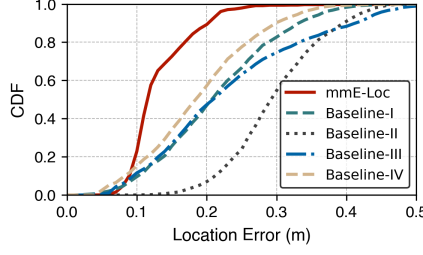


Fig. 15. Outdoor accuracy comparison

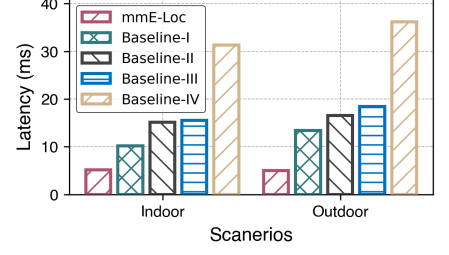


Fig. 16. Latency comparison

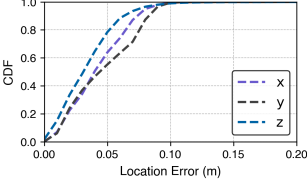


Fig. 17. Error along the x-, y-, and z-axes during standard flight

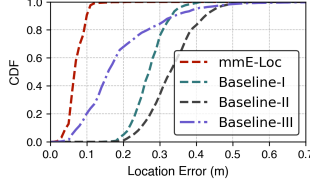


Fig. 18. Error during a standard flight (near-distance setting)

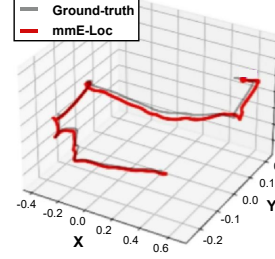


Fig. 19. Flight trajectory

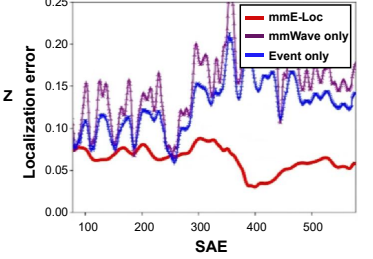


Fig. 20. Localization error

processing. The RTK localization results served as the ground truth for our outdoor tests.

Comparative methods. (i) *Baseline-I* [44]: a SOTA point cloud-based drone localization system using single-chip mmWave radar, which is a ground localization system. (ii) *Baseline-II* [43]: a SOTA single event camera-based drone ground localization system applies to drones with known geometries. The original method for onboard obstacle localization lacks public code. We implement its monocular 3D localization module for *ground-based* drone localization, excluding ego-motion compensation for noise reduction. (iii) *Baseline-III* [43]: a SOTA dual event camera-based drone localization system. The original method uses onboard stereo event cameras for obstacle localization, but its code is unavailable. We implement its stereo 3D location estimation module, excluding ego-motion compensation, for *ground-based* drone localization. (iii) *Baseline-IV* [56]: a SOTA deep learning-based object localization system utilizes monocular images and mmWave point clouds as input, harnessing the complementary information from both the radar and camera. We pre-train neural networks and apply a Kalman Filter to adapt original method for *ground-based* 3D drone localization.

Evaluation metrics. mmE-Loc provides continuous, low-latency location estimates, ensuring accurate and responsive drone localization. Similar to related works, we evaluate location estimation error in meters and processing latency in milliseconds, facilitating direct comparison with existing methods in terms of both accuracy and efficiency.

Robustness experiments. During drone landing, localization may occur under varying lighting conditions. To assess mmE-Loc's adaptability, we conduct experiments across diverse scenarios, including different environments, drone models, lighting conditions (Fig.13a-f), and background dynamics (e.g., moving objects like balls). We also evaluate the impact of distance, occlusions (e.g., partial obstruction of the drone in event camera's FoV), and velocity to demonstrate robustness. Baseline-IV is excluded from comparison due to its high latency from the frame camera's exposure time.

B. Overall performance

Drone localization. Fig.14 shows the localization performance of mmE-Loc in an indoor environment using a DJI Mini 3 Pro drone, compared to four baselines. mmE-Loc achieves an average end-to-end localization error of $0.083m$, outperforming the baselines with errors of $0.261m$, $0.345m$, $0.209m$, and $0.160m$, making it well-suited for landing assistance. Fig.15b presents mmE-Loc's localization performance in an outdoor setting with a DJI M30T drone. Here, mmE-Loc achieves the lowest average error of $0.135m$, outperforming the baselines by 39.2%, 56.0%, 43.8%, and 31.8%, respectively. Baseline-I suffers from point cloud errors caused by phase center offset, resulting in deviations from the drone's geometric center. In indoor environments, these errors are exacerbated by specular reflections, diffraction, and multipath effects that further degrade radar measurements. Baseline-II employs a single event camera with prior knowledge of drone geometry, while Baseline-III uses a stereo setup with dual event cameras for depth estimation. Both approaches are vulnerable to environmental noise (e.g., birds), which can lead to inaccurate depth estimation. Baseline-IV relies on deep learning models, which may exhibit higher errors when deployed in unseen environments due to limited generalization. In contrast, mmE-Loc significantly improves performance by leveraging the complementary strengths of radar and event cameras. It operates without the need for pre-training, enabling robust and broadly applicable localization.

End-to-end latency. We evaluate end-to-end latency, including the *CCT* and *GAJO* phases. As shown in Fig.16, mmE-Loc achieves $5.12ms$ latency indoors, outperforming four baselines at $10.19ms$, $15.12ms$, $15.52ms$, and $31.2ms$, respectively. In outdoor scenarios with higher complexity, baseline latencies increase, and mmE-Loc maintains the lowest latency, outperforming them by 62.5%, 69.6%, 72.7%, and 83.3%. Baselines face increased latency due to environmental noise and more optimization parameters. mmE-Loc establishes a tight coupling between the event camera and mmWave radar. It incorporates *CCT* module to exploit temporal consistency,

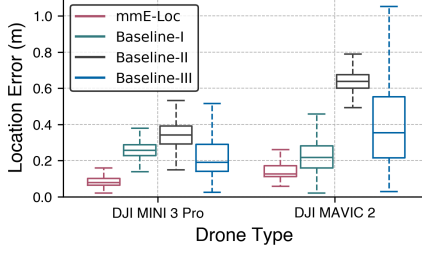


Fig. 21. Impact of drone type

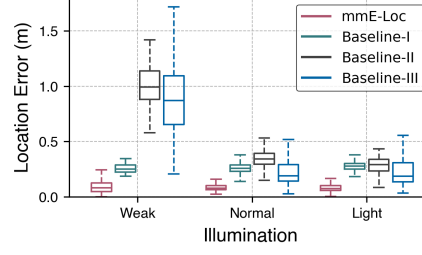


Fig. 22. Impact of env. & illu.

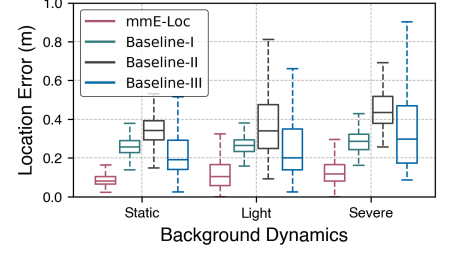


Fig. 23. Impact of background

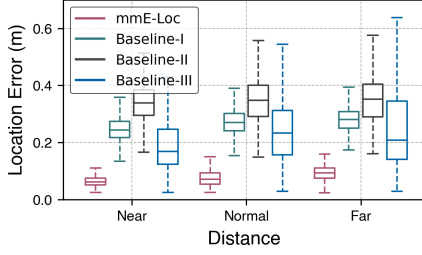


Fig. 24. Impact of distance

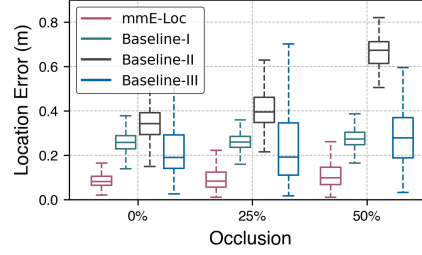


Fig. 25. Impact of occlusion

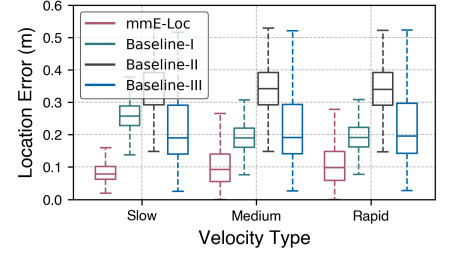


Fig. 26. Impact of velocity

drone's periodic micro-motions and structure for drone detection. Then, *GAJO* module, combined with an incremental optimization approach, enhances spatial complementarity while minimizing system latency.

Typical flight performance. To validate the performance of mmE-Loc, we present the error analysis during a typical flight. Fig.17 illustrates the error distribution along the x-, y-, and z-axes throughout the flight, while Fig.18 focuses on errors in a near-distance scenario. mmE-Loc achieves low errors across all three dimensions and consistently outperforms the baselines. Moreover, Fig.19 shows the drone's flight trajectory compared to the ground-truth path, demonstrating that mmE-Loc's estimated trajectory closely matches the ground-truth path. Fig.20 depicts error over time, indicating that mmE-Loc maintains consistently low errors throughout flight.

C. System robustness evaluation

To demonstrate the versatility and robustness of mmE-Loc, we conduct experiments under various conditions.

Impact of drone type. We evaluate the impact of different drone types under controlled indoor conditions, using a DJI Mini 3 Pro (Fig.13c) and a DJI Mavic 2 (Fig.13d), the results are presented in Fig.21. The average error results demonstrate that mmE-Loc outperforms all baselines when using DJI Mini 3 Pro. For DJI Mavic 2, Baseline-II and Baseline-III exhibit larger localization errors, primarily due to changes in drone's geometry that impact depth estimation. mmE-Loc's localization error of $0.135m$ remains within an acceptable range, which outperforms all baselines with $0.222m$, $0.639m$, and $0.403m$, demonstrating its effectiveness across drone types.

Impact of environment & illumination. The performance of mmE-Loc in different environments with varying lighting conditions (Fig.13e and Fig.13f) is shown in Fig.22. Although event cameras offer a high dynamic range, the events generated by drones are still influenced by illumination conditions. As lighting diminishes, Baseline-II and Baseline-III suffer from increased localization errors due to degraded depth estimation performance. In comparison, mmE-Loc sustains a relatively

low average error even under low illumination, recording an average error of $0.103m$ and a maximum error of $0.27m$. mmE-Loc's consistent performance across different lighting conditions, without requiring pre-training or prior knowledge, makes it a versatile solution.

Impact of background motion. We test mmE-Loc with dynamic background motion, as shown in Fig.23. The intensity of dynamic background motion is controlled by deploying other moving objects in the scene (e.g., balls). All baselines show higher localization errors with increasing background motion due to misidentification of the radar and camera. Despite this, mmE-Loc maintains an average error of $0.129m$ in the most challenging scenarios. This is achieved through mmE-Loc's consistency-instructed measurement filter, which uses the drone's physical knowledge of periodic micro-motions and structure to distinguish it from other objects.

Impact of distance. We investigate the impact of drone-to-platform distance indoors with a DJI Mini 3 Pro ($0.25m \times 0.36m \times 0.07m$). Fig.24 shows the results, categorized into Near ($< 3m$), Normal ($3m \sim 6m$), and Far ($> 6m$) distances. As distance increases, all methods show higher errors. mmE-Loc achieves an average error of $0.102m$ for far distances, outperforming other baselines. mmE-Loc combines mmWave radar for depth sensing with an event camera for high-resolution 2D imaging, effectively addressing the low spatial resolution of mmWave radar and the scale ambiguity of event cameras. Recognizing the critical need for precise landings, mmE-Loc serves as a complementary system to existing solutions. When integrated with RTK and visual markers, it enhances localization reliability and accuracy in real-world applications.

Impact of occlusion. We validate mmE-Loc's robustness with partially occluded drones. Occlusion is introduced by partially obstructing the drone within the event camera's field of view, including cases where the drone appears only partially in FoV. Fig.25 shows that with 25% occlusions, mmE-Loc maintains high performance with an average error of $0.094m$.

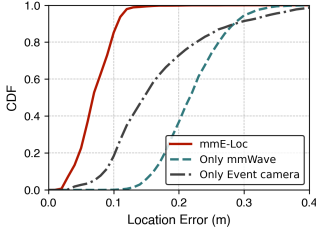


Fig. 27. Effectiveness of sensor fusion

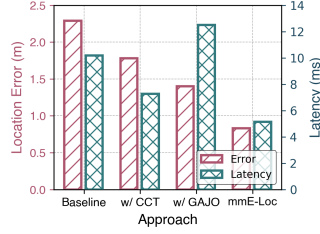


Fig. 28. Impact of different modules

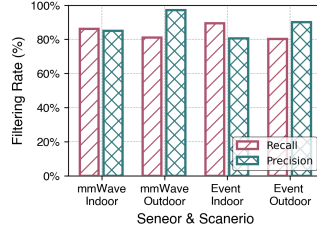


Fig. 29. Performance of CCT

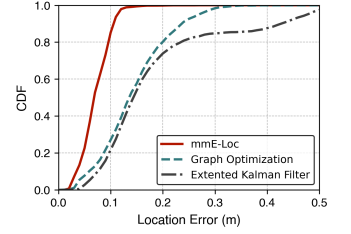


Fig. 30. Performance of GAJO

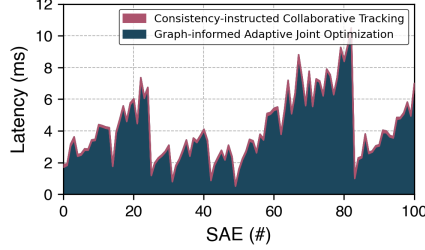


Fig. 31. System latency

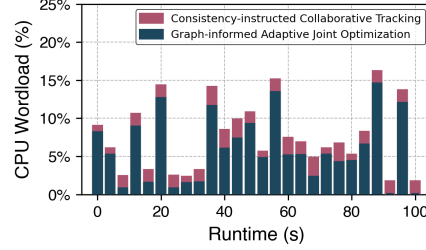


Fig. 32. CPU workload

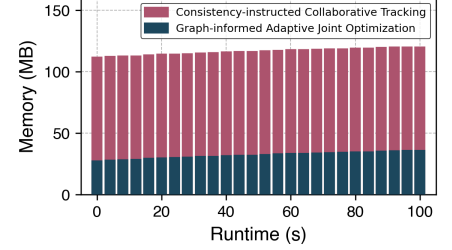


Fig. 33. Memory usage

At 50% occlusion, the average error of mmE-Loc increases to $0.12m$. Baseline-II and -III show larger errors due to incorrect depth estimation caused by occlusion. Therefore, mmE-Loc harnesses the strengths of both modalities in accurately tracking the drone's location, even under partial occlusion.

Impact of drone velocity. We further evaluate mmE-Loc's robustness under different drone velocities in Fig.26. Velocities are categorized as slow ($v < 0.5m/s$), medium ($0.5m/s \leq v < 1m/s$), and rapid ($1m/s \leq v < 1.5m/s$), corresponding to various drone landing stages. Although errors of all methods increased with speed, mmE-Loc maintained an average error of $0.11m$ even in rapid speed scenarios, outperforming baselines by 44%, 68.5%, and 52.4%. This benefit stems from the high sampling rates of both the event camera and mmWave radar, which enable more frequent observations of the drone, including both 2D imaging and depth measurements.

D. Ablation study

We experimentally analyze the core components of mmE-Loc, focusing on both their individual performance and the improvements they contribute to the overall system.

Effectiveness of multi-modal fusion. We demonstrate the superiority of fusing radar and event cameras over using each sensor individually. Fig.27 shows that the fusion-based approach significantly outperforms both radar-only and event camera-only methods in terms of location error. mmE-Loc outperforms event-only approach by 63.6% and exceeds radar-only method by 52.9%.

Contributions of each module. We investigate the contributions of CCT and GAJO to mmE-Loc by gradually integrating them with the event camera into the baseline system (i.e., the radar only-based method) and assessing localization accuracy and end-to-end latency. Fig.28 illustrates that without these modules, the baseline method achieves a localization error of $0.229m$ and latency of $10.19ms$. Integrating the event camera with the CCT module reduces the localization error to $0.178m$ and decreases latency to $7.27ms$. This is because

the event camera, together with the CCT module, filters out the noisy point cloud generated by the radar. Integrating the event camera with GAJO further reduces the error to $0.139m$, although the delay increases due to the absence of an efficient detection mechanism. This is because the GAJO jointly optimize multiple locations to improve accuracy; however, without a robust detection strategy, the system may also optimize the locations of non-drone objects, leading to additional computational overhead. Finally, integrating both CCT and GAJO minimizes both the error and latency.

Performance of CCT. We test CCT's filtering performance on mmWave and event data in both indoor and outdoor scenarios. In Fig.29, higher recall signifies more drone-triggered events preserved, while higher precision indicates more background events removed. In indoor conditions, CCT achieves recalls over 86% for mmWave and 89% for event, with precision above 85% and 80%, respectively. In outdoor conditions, recall and precision remain above 80% for both types, demonstrating CCT's effectiveness. This is because the CCT module effectively leverages the complementary characteristics of the two sensing modalities, while also utilizing drone's physical knowledge of periodic micro-motions and structure to distinguish drone from other objects.

Performance of GAJO. We compare the performance of different multi-modal fusion strategies. Specifically, we evaluate mmE-Loc against two widely used approaches: the extended Kalman filter (EKF) and Graph Optimization (GO). As shown in Fig.30, mmE-Loc enhances localization performance by over 57.9% compared to EKF and 47.1% compared to GO, due to its tightly coupled multi-modal fusion and the incremental optimization method.

E. System efficiency study

The mmE-Loc distinguishes itself from existing models and learning-based methods due to its low latency and minimal resource overhead. Fig.31 presents the end-to-end latency of the typical localization process, which includes delays from both CCT and GAJO modules. During drone localization,

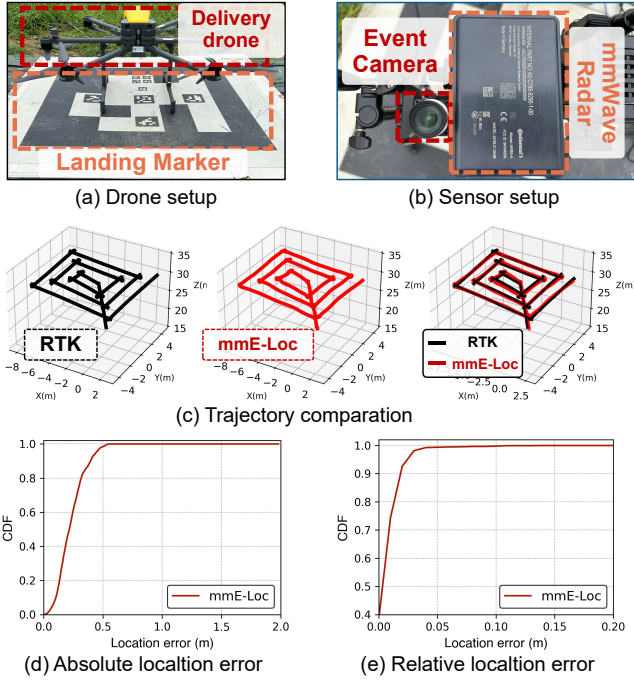


Fig. 34. Case study: delivery drone airport.

mmE-Loc's latency may vary because its motion-aware adaptive optimization scheme optimizes different sets of locations at different times, and the incremental optimization method dynamically decides whether to perform incremental or full optimization at each time step. As the size of the location set increases, the optimization time also grows. Nevertheless, thanks to the motion-aware adaptive optimization scheme and the incremental optimization method, mmE-Loc maintains low latency overall. Nonetheless, mmE-Loc's latency remains suitable for use in flight control loops. Fig.32 and Fig.33 indicate that CPU usage doesn't exceed 18%, with memory usage under 120MB. Meanwhile, memory usage slightly increases as the location set size grows.

VI. CASE STUDY

A. Landing at real-world drone airport

As shown in Fig.34a, to verify the system's usability, we conduct an experiment using a custom drone equipped with six propellers and managed by a PX4 flight controller. This drone is developed by a world-class delivery company exploring the feasibility of instant deliveries. The experiment takes place at a real-world delivery drone airport. To enable drone localization over a larger area, we employ an ARS548 mmWave radar, as depicted in Fig.34b. Fig.34c, Fig.34d, and Fig.34e illustrate the localization results as the drone follows a square spiral trajectory at an altitude of 30 m. In the qualitative analysis, the left image in Fig.34c shows the localization results from RTK, while the middle image presents the results from mmE-Loc. As illustrated in the right image of Fig.34c, mmE-Loc produces smooth trajectories that closely align with those of RTK, demonstrating its potential to complement RTK-based localization. In the quantitative analysis, the results in Fig.34d and Fig.34e show that in real-world scenarios, mmE-Loc achieves high localization precision, maintaining a maximum

absolute location error error below 0.5m and relative location error error below 0.1m. mmE-Loc has significant potential as a complementary system to RTK, aiding drone in challenging environments (e.g., urban canyons, where RTK may be compromised by signal blockage).

VII. RELATED WORK

Drone ground localization. Drones have been widely applied in various scenarios [57]–[59]. Several types of work have been proposed to assist drones in localization. (i) *Satellite-based systems.* The Global Positioning System (GPS) provides *m*-level accuracy outdoors [60], [61], while Real-Time Kinematic (RTK) achieves *cm*-level precision but is costly. However, these satellite-based systems struggle in urban canyons [62], [63]. (ii) *Optics-based systems.* These systems, such as motion capture, offer *cm*-level accuracy indoors but require precise calibration, making them impractical for outdoor use [64]. (iii) *Compact mobile sensor-based systems.* To address these issues, various sensor-based techniques are proposed, including camera [65]–[68], radar [27], [28], LiDAR [69]–[72] and acoustic [4] often combined with SLAM (Simultaneous Localization and Mapping) [29], [73], [74] or deep learning algorithms [75]–[78], aim to improve drone localization. However, the limited spatio-temporal resolution of these sensors hinders precise, low-latency localization required for accurate drone landings. For instance, cameras and LiDARs typically operate at low frame rates (below 50Hz), which may fail to capture rapid motion between frames, thereby reducing localization accuracy [79]. Acoustic signal-based systems are highly vulnerable to environmental noise, with even the presence of nearby humans significantly affecting their stability. Visual marker-based systems, which rely on downward-facing cameras mounted on drones, are also sensitive to lighting conditions due to the limited dynamic range of conventional frame-based cameras.

Compared to previous methods, mmE-Loc introduces a novel sensor configuration that combines an event camera with mmWave radar, leveraging their ultra-high sampling rates to achieve high-accuracy ground localization for drones with low latency. Additionally, mmE-Loc is resistant to lighting variations thanks to its sensor design: event cameras provide a high dynamic range, while mmWave radar, being based on radio waves, is inherently unaffected by lighting conditions. It is important to emphasize that mmE-Loc is designed to complement, not replace, existing localization solutions. To ensure precise landings, mmE-Loc can be integrated with RTK and visual marker systems, delivering a more reliable and accurate localization service.

mmWave radar for localization and tracking. Millimeter-wave is highly sensitive and more accurate due to its mm-level wavelength. mmWave radar offers high sensitivity and precision due to its sub-millimeter wavelength [25], [80], [81]. Several mmWave radar-based solutions for drone ground localization combine signal intensity methods, but face challenges in accurately tracking the drone's center [48], [82], [83]. This difficulty arises from the drone's large size (e.g., 80 cm across), causing it to appear as a non-uniform blob

in radar returns. Additionally, these methods often produce unstable results with frequent outliers, as multipath scattering can obscure the main signal and low spatial resolution of radar [84]. Other approaches leverage deep learning-based methods but require extensive pre-modeling and neural network training for each drone model [29], [85], [86]. These methods tend to struggle with tracking different drone models and perform poorly in environments not represented in training dataset. Several solutions integrate visual sensors to assist radar [56], [87], [88]. However, these approaches introduce latency due to exposure times and image processing delays.

To address the challenges of accuracy and latency, we replace traditional RGB cameras with event cameras and pair them with mmWave radar, significantly enhancing overall system performance. By leveraging temporal consistency of both modalities along with the drone's physical knowledge of periodic micro-motions and structure through the proposed *CCT* module, mmE-Loc achieves high-precision tracking without requiring any prior knowledge (e.g., training data or 3D models). The integration of the *GAJO* module further improves ground localization accuracy by exploiting spatial complementarity. Additionally, by incorporating drone's motion as a constrain, we introduce a motion-aware adaptive optimization scheme that reduces the computation time during optimization. Moreover, in our implementation, we design an incremental optimization method that further brings the localization latency down to the millisecond level.

Sensor fusion techniques. Sensor fusion techniques are widely used in localization [89]–[92]. (i) *Traditional pipeline-based fusion methods.* These approaches typically integrate dense point clouds from sensors (e.g., LiDAR) to provide depth information, alongside pixel data from frame cameras [93], [94]. However, these methods are generally limited to fusing two types of dense measurements and cannot directly accommodate the sparse data output from event cameras and mmWave radar. (ii) *Deep learning-based fusion methods.* Recent advancements have explored learning-based methods for fusing mmWave radar, frame cameras, and IMUs for localization [95], [96]. While these methods offer promising results, they often require extensive labeled training data and experience performance degradation in dynamic environments [29], [56], [97]–[99]. In contrast, mmE-Loc employs a tightly coupled fusion framework that uses factor graphs and an incremental optimization method to jointly refine radar and event-based tracking models. Additionally, mmE-Loc incorporates the drone's motion information as a trigger to dynamically adjust both the optimization frequency and the size of the location set to be optimized, further reducing computational overhead. Compared to deep learning-based approaches, this method offers a more transparent probabilistic interpretation, enhancing both efficiency and explainability.

VIII. DISCUSSION

How does mmE-Loc relate to visual markers? Currently, delivery drones utilize visual markers and onboard cameras for self-localization. In contrast, mmE-Loc focuses on ground-based drone localization, enabling the landing pad to determine

the spatial relationship between the drone and itself for precise adjustments. In practice, mmE-Loc operates alongside visual markers to enhance reliability of localization service.

Is it feasible to design an onboard sensor system for drone landing localization? It's theoretically feasible. However, designing an onboard system for drone localization using an event camera and mmWave radar presents several challenges. Given the continuous motion of the drone, the system must address: (i) motion compensation for event data, (ii) reliable feature extraction and matching within the event stream despite its lack of semantic information, and (iii) the sparsity of radar measurements and noise induced by specular reflections, diffraction, and multi-path effects.

How does network latency impact the system, and how can potential delay-related issues be addressed? mmE-Loc is designed to assist ground platforms in locating drones and guiding them to land accurately at designated spots. Network latency may impact the location update rate for the drone. To mitigate this issue, drone airports usually deploy access points near the landing pad and utilize multiple wireless links, including Wi-Fi and cellular networks, to ensure reliable and fast communication. Additionally, an optics-based communication system could be integrated into the system to ensure a high communication frequency [100].

IX. CONCLUSION

This paper presents a novel sensor configuration that combines an event camera with mmWave radar, synchronizing their ultra-high sampling frequencies to enable mmE-Loc, a ground localization system designed for drone landings, achieving centimeter-level accuracy and millisecond-level latency. mmE-Loc comprises two key components: (i) the consistency-instructed collaborative tracking (CCT) module, which exploits cross-modal temporal consistency along with the drone's physical knowledge of periodic micro-motions and structure to enable precise drone detection; and (ii) the graph-informed adaptive joint optimization (GAJO) module, which enhances localization accuracy and reduces latency by leveraging cross-modal spatial complementarity. This module also incorporates the drone's motion information to dynamically adjust the optimization timing and the size of the location set to be optimized, further minimizing computational overhead. Extensive evaluations across diverse scenarios validate the effectiveness and robustness of mmE-Loc.

REFERENCES

- [1] Haoyang Wang, Jingao Xu, Xinyu Luo, Xuecheng Chen, Ting Zhang, Ruiyang Duan, Yunhao Liu, and Xinlei Chen. Ultra-high-frequency harmony: mmwave radar and event camera orchestrate accurate drone landing. In *Proceedings of the 23rd ACM Conference on Embedded Networked Sensor Systems*, pages 15–29, 2025.
- [2] Hong kong can succeed in developing a thriving low-altitude economy. <https://www.chinadailyhk.com/hk/article/593176>.
- [3] Xuecheng Chen, Haoyang Wang, Yuhao Cheng, Haohao Fu, Yuxuan Liu, Fan Dang, Yunhao Liu, Jinqiang Cui, and Xinlei Chen. Ddl: Empowering delivery drones with large-scale urban sensing capability. *IEEE Journal of Selected Topics in Signal Processing*, 2024.
- [4] Weiguo Wang, Luca Mottola, Yuan He, Jinming Li, Yimiao Sun, Shuai Li, Hua Jing, and Yulei Wang. Micnest: Long-range instant acoustic localization of drones in precise landing. In *Proceedings of the 20th ACM SenSys*, pages 504–517, 2022.

- [5] Xuecheng Chen, Haoyang Wang, Zuxin Li, Wenbo Ding, Fan Dang, Chenye Wu, and Xinlei Chen. Deliversense: Efficient delivery drone scheduling for crowdsensing with deep reinforcement learning. In *Proceedings of the 2022 ACM International Joint Conference and 2022 International Symposium on Pervasive and Ubiquitous Computing and Wearable Computers*, 2022.
- [6] Yuan He, Weiguo Wang, Luca Mottola, Shuai Li, Yimiao Sun, Jinming Li, Hua Jing, Ting Wang, and Yulei Wang. Acoustic localization system for precise drone landing. 2023.
- [7] Susu Xu, Xinlei Chen, Xidong Pi, Carlee Joe-Wong, Pei Zhang, and Hae Young Noh. Vehicle dispatching for sensing coverage optimization in mobile crowdsensing systems. In *Proceedings of the 18th International Conference on Information Processing in Sensor Networks*, pages 311–312, 2019.
- [8] Jingao Xu, Hao Cao, Zheng Yang, Longfei Shangguan, Jialin Zhang, Xiaowu He, and Yunhao Liu. {SwarmMap}: Scaling up real-time collaborative visual {SLAM} at the edge. In *19th USENIX Symposium on Networked Systems Design and Implementation (NSDI 22)*, pages 977–993, 2022.
- [9] Xinlei Chen, Susu Xu, Xinyu Liu, Xiangxiang Xu, Hae Young Noh, Lin Zhang, and Pei Zhang. Adaptive hybrid model-enabled sensing system (hmss) for mobile fine-grained air pollution estimation. *IEEE Transactions on Mobile Computing*, 2020.
- [10] Jiayuan Ren, Yanggang Xu, Zuxin Li, Chaopeng Hong, Xiao-Ping Zhang, and Xinlei Chen. Scheduling uav swarm with attention-based graph reinforcement learning for ground-to-air heterogeneous data communication. In *Adjunct Proceedings of the 2023 ACM International Joint Conference on Pervasive and Ubiquitous Computing & the 2023 ACM International Symposium on Wearable Computing*, pages 670–675, 2023.
- [11] Jingao Xu, Mihir Bala, Thomas Eiszler, Xiangliang Chen, Qifei Dong, Aditya Chananana, Padmanabhan Pillai, and Mahadev Satyanarayanan. Terraslam: Towards gps-denied localization. In *Proceedings of the ACM MobiSys*, 2025.
- [12] Xuecheng Chen, Zijian Xiao, Yuhua Cheng, ChenChun Hsia, Haoyang Wang, Jingao Xu, Susu Xu, Fan Dang, Xiao-Ping Zhang, Yunhao Liu, et al. Soscheduler: Toward proactive and adaptive wildfire suppression via multi-uav collaborative scheduling. *IEEE Internet of Things Journal*, 2024.
- [13] Bin-Bin Zhang, Dongheng Zhang, Ruiyuan Song, Binqun Wang, Yang Hu, and Yan Chen. RF-search: Searching unconscious victim in smoke scenes with rf-enabled drone. In *Proceedings of the 29th Annual International Conference on Mobile Computing and Networking*, pages 1–15, 2023.
- [14] Yanggang Xu, Jirong Zha, Jiayuan Ren, Xintao Jiang, Hongfei Zhang, and Xinlei Chen. Scalable multi-agent reinforcement learning for effective uav scheduling in multi-hop emergency networks. In *Proceedings of the 30th Annual International Conference on Mobile Computing and Networking*, pages 2028–2033, 2024.
- [15] Yuan He, Weiguo Wang, Luca Mottola, Shuai Li, Yimiao Sun, Jinming Li, Hua Jing, Ting Wang, and Yulei Wang. Acoustic localization system for precise drone landing. *IEEE Transactions on Mobile Computing*, 23(5):4126–4144, 2023.
- [16] Yimiao Sun, Weiguo Wang, Luca Mottola, Ruijin Wang, and Yuan He. Aim: Acoustic inertial measurement for indoor drone localization and tracking. In *Proceedings of the 20th ACM SenSys*, pages 476–488, 2022.
- [17] Javier González-Trejo, Diego Mercado-Ravell, Israel Becerra, and Rafael Murrieta-Cid. On the visual-based safe landing of uavs in populated areas: a crucial aspect for urban deployment. *IEEE Robotics and Automation Letters*, 6(4):7901–7908, 2021.
- [18] Yiming Li, Markus Mund, Philipp Hoess, Joran Deschamps, Ulf Matti, Bianca Nijmeijer, Vilma Jimenez Sabinina, Jan Ellenberg, Ingmar Schoen, and Jonas Ries. Real-time 3d single-molecule localization using experimental point spread functions. *Nature methods*, 15(5):367–369, 2018.
- [19] Stephen Xia, Minghui Zhao, Charuvahan Adhivaran, Kaiyuan Hou, Yuyang Chen, Jingping Nie, Eugene Wu, Karthik Dantu, and Xiaofan Jiang. Anemoi: A low-cost sensorless indoor drone system for automatic mapping of 3d airflow fields. In *Proceedings of the 29th Annual International Conference on Mobile Computing and Networking*, pages 1–16, 2023.
- [20] Haotian Zhang, Gaoang Wang, Zhichao Lei, and Jenq-Neng Hwang. Eye in the sky: Drone-based object tracking and 3d localization. In *Proceedings of the 27th ACM international conference on multimedia*, pages 899–907, 2019.
- [21] Jinrui Zhang, Huan Yang, Ju Ren, Deyu Zhang, Bangwen He, Ting Cao, Yuanchun Li, Yaoxue Zhang, and Yunxin Liu. Mobidepth: Real-time depth estimation using on-device dual cameras. In *Proceedings of the 28th ACM MobiCom*, pages 528–541, 2022.
- [22] Zhiyuan Xie, Xiaomin Ouyang, Li Pan, Wenrui Lu, Guoliang Xing, and Xiaoming Liu. Mozart: A mobile to system for sensing in the dark through phase manipulation. In *Proceedings of the 21st Annual International Conference on Mobile Systems, Applications and Services*, pages 163–176, 2023.
- [23] Yunfan Zhang, Tim Scargill, Ashutosh Vaishnav, Gopika Premsankar, Mario Di Francesco, and Maria Gorlatova. Indepth: Real-time depth inpainting for mobile augmented reality. *Proc. ACM Interact. Mob. Wearable Ubiquitous Technol.*, 6(1), March 2022.
- [24] Kaikai Deng, Dong Zhao, Qiaoyue Yan, Shuyue Wang, Zihan Zhang, Anfu Zhou, and Huadong Ma. Geryon: Edge assisted real-time and robust object detection on drones via mmwave radar and camera fusion. *Proceedings of the ACM on Interactive, Mobile, Wearable and Ubiquitous Technologies*, 6(3):1–27, 2022.
- [25] Chris Xiaoxuan Lu, Stefano Rosa, Peijun Zhao, Bing Wang, Changhao Chen, John A. Stankovic, Niki Trigoni, and Andrew Markham. See through smoke: Robust indoor mapping with low-cost mmwave radar, 2020.
- [26] Jia Zhang, Xin Na, Rui Xi, Yimiao Sun, and Yuan He. mmhawkkey: Passive uav detection with a cots mmwave radar. In *2023 20th Annual IEEE International Conference on Sensing, Communication, and Networking (SECON)*, pages 267–275. IEEE, 2023.
- [27] Emerson Sie, Zikun Liu, and Deepak Vasisht. Batmobility: Towards flying without seeing for autonomous drones. In *Proceedings of the 29th ACM MobiCom*, pages 1–16, 2023.
- [28] Tatsuya Iizuka, Takuya Sasatani, Toru Nakamura, Naoko Kosaka, Masaki Hisada, and Yoshihiro Kawahara. Millisign: mmwave-based passive signs for guiding uavs in poor visibility conditions. In *Proceedings of the 29th ACM MobiCom*, pages 1–15, 2023.
- [29] Chris Xiaoxuan Lu, Stefano Rosa, Peijun Zhao, Bing Wang, Changhao Chen, John A. Stankovic, Niki Trigoni, and Andrew Markham. See through smoke: robust indoor mapping with low-cost mmwave radar. In *Proceedings of the 18th ACM MobiSys*, pages 14–27, 2020.
- [30] Chris Xiaoxuan Lu, Muhammad Risqi U Saputra, Peijun Zhao, Yasin Almalioglu, Pedro PB De Gusmao, Changhao Chen, Ke Sun, Niki Trigoni, and Andrew Markham. milliego: single-chip mmwave radar aided egomotion estimation via deep sensor fusion. In *Proceedings of the 18th ACM SenSys*, pages 109–122, 2020.
- [31] Zhuoqun Cheng, Richard West, and Craig Einstein. End-to-end analysis and design of a drone flight controller. *IEEE Transactions on Computer-Aided Design of Integrated Circuits and Systems*, 37(11):2404–2415, 2018.
- [32] Emerson Sie, Zikun Liu, and Deepak Vasisht. Batmobility: Towards flying without seeing for autonomous drones. In *Proceedings of the 29th Annual International Conference on Mobile Computing and Networking*, ACM MobiCom '23, New York, NY, USA, 2023. Association for Computing Machinery.
- [33] Haoyang Wang, Ruishan Guo, Pengtao Ma, Ciyu Ruan, Xinyu Luo, Wenhua Ding, Tianyang Zhong, Jingao Xu, Yunhao Liu, and Xinlei Chen. Towards mobile sensing with event cameras on high-agility resource-constrained devices: A survey. *arXiv preprint arXiv:2503.22943*, 2025.
- [34] Guillermo Gallego, Tobi Delbrück, Garrick Orchard, Chiara Bartolozzi, Brian Taba, Andrea Censi, Stefan Leutenegger, Andrew J Davison, Jörg Conradt, Kostas Daniilidis, et al. Event-based vision: A survey. *IEEE transactions on pattern analysis and machine intelligence*, 44(1):154–180, 2020.
- [35] Ciyu Ruan, Chenyu Zhao, Chenxin Liang, Xinyu Luo, Jingao Xu, and Xinlei Chen. Distill drops into data: Event-based rain-background decomposition network. In *Proceedings of the 30th Annual International Conference on Mobile Computing and Networking*, pages 2072–2077, 2024.
- [36] Botao He, Ze Wang, Yuan Zhou, Jingxi Chen, Chahat Deep Singh, Haojia Li, Yuman Gao, Shaojie Shen, Kaiwei Wang, Yanjun Cao, et al. Microsaccade-inspired event camera for robotics. *Science Robotics*, 9(90):eadj8124, 2024.
- [37] Ciyu Ruan, Ruishan Guo, Zihang Gong, Jingao Xu, Wenhan Yang, and Xinlei Chen. Pre-mamba: A 4d state space model for ultra-high-frequency event camera deraining. *arXiv preprint arXiv:2505.05307*, 2025.
- [38] Xinyu Luo, Haoyang Wang, Ciyu Ruan, Chenxin Liang, Jingao Xu, and Xinlei Chen. Eventtracker: 3d localization and tracking of high-speed object with event and depth fusion. In *Proceedings of the 30th Annual*

- International Conference on Mobile Computing and Networking*, pages 1974–1979, 2024.
- [39] Zhongping Cao, Guangyu Mei, Xuemei Guo, and Guoli Wang. Virteach: mmwave radar point cloud based pose estimation with virtual data as a teacher. *IEEE Internet of Things Journal*, 2024.
 - [40] Hankai Liu, Xiulong Liu, Xin Xie, Xinyu Tong, and Keqiu Li. Pmtrack: Enabling personalized mmwave-based human tracking. *Proceedings of the ACM on Interactive, Mobile, Wearable and Ubiquitous Technologies*, 7(4):1–30, 2024.
 - [41] Ziwei Wang, Yonhon Ng, Cedric Scheerlinck, and Robert Mahony. An asynchronous kalman filter for hybrid event cameras. In *Proceedings of the IEEE/CVF International Conference on Computer Vision*, pages 448–457, 2021.
 - [42] Ignacio Alzugaray and Margarita Chli. Asynchronous corner detection and tracking for event cameras in real time. *IEEE Robotics and Automation Letters*, 3(4):3177–3184, 2018.
 - [43] Davide Falanga, Kevin Kleber, and Davide Scaramuzza. Dynamic obstacle avoidance for quadrotors with event cameras. *Science Robotics*, 5(40):eaaz9712, 2020.
 - [44] Peijun Zhao, Chris Xiaoxuan Lu, Bing Wang, Niki Trigoni, and Andrew Markham. 3d motion capture of an unmodified drone with single-chip millimeter wave radar. In *2021 IEEE International Conference on Robotics and Automation (ICRA)*, pages 5186–5192. IEEE, 2021.
 - [45] Anton Mitrokhin, Cornelia Fermüller, Chethan Parameshwara, and Yiannis Aloimonos. Event-based moving object detection and tracking. In *2018 IEEE/RSJ International Conference on Intelligent Robots and Systems (IROS)*, pages 1–9. IEEE, 2018.
 - [46] Yingqi Wang, Zhongqin Wang, J Andrew Zhang, Haimin Zhang, and Min Xu. Vital sign monitoring in dynamic environment via mmwave radar and camera fusion. *IEEE Transactions on Mobile Computing*, 2023.
 - [47] Zhe Min, Jiaole Wang, and Max Q-H Meng. Joint rigid registration of multiple generalized point sets with anisotropic positional uncertainties in image-guided surgery. *IEEE Transactions on Automation Science and Engineering*, 19(4):3612–3627, 2021.
 - [48] Kun Qian, Zhaoyuan He, and Xinyu Zhang. 3d point cloud generation with millimeter-wave radar. *Proceedings of the ACM on Interactive, Mobile, Wearable and Ubiquitous Technologies*, 4(4):1–23, 2020.
 - [49] Guidong Zhang, Guoxuan Chi, Yi Zhang, Xuan Ding, and Zheng Yang. Push the limit of millimeter-wave radar localization. *ACM Transactions on Sensor Networks*, 19(3):1–21, 2023.
 - [50] Shijie Lin, Fang Xu, Xuhong Wang, Wen Yang, and Lei Yu. Efficient spatial-temporal normalization of sae representation for event camera. *IEEE Robotics and Automation Letters*, 5(3):4265–4272, 2020.
 - [51] Jirong Zha, Yuxuan Fan, Kai Li, Han Li, Chen Gao, Xinlei Chen, and Yong Li. Dimm: Decoupled multi-hierarchy kalman filter for 3d object tracking. *arXiv preprint arXiv:2505.12340*, 2025.
 - [52] Carlos Campos, Richard Elvira, Juan J Gómez Rodríguez, José MM Montiel, and Juan D Tardós. Orb-slam3: An accurate open-source library for visual, visual-inertial, and multimap slam. *IEEE Transactions on Robotics*, 37(6):1874–1890, 2021.
 - [53] Christian H Bischof and Gregorio Quintana-Ortí. Computing rank-revealing qr factorizations of dense matrices. *ACM Transactions on Mathematical Software (TOMS)*, 24(2):226–253, 1998.
 - [54] Michael Kaess, Ananth Ranganathan, and Frank Dellaert. isam: Incremental smoothing and mapping. *IEEE Transactions on Robotics*, 24(6):1365–1378, 2008.
 - [55] Michael Kaess, Hordur Johannsson, Richard Roberts, Violella Ila, John J Leonard, and Frank Dellaert. isam2: Incremental smoothing and mapping using the bayes tree. *The International Journal of Robotics Research*, 31(2):216–235, 2012.
 - [56] Xian Shuai, Yulin Shen, Yi Tang, Shuyao Shi, Luping Ji, and Guoliang Xing. millieye: A lightweight mmwave radar and camera fusion system for robust object detection. In *Proceedings of the International Conference on Internet-of-Things Design and Implementation*, pages 145–157, 2021.
 - [57] Yuxuan Liu, Haoyang Wang, Fanhang Man, Jingao Xu, Fan Dang, Yunhao Liu, Xiao-Ping Zhang, and Xinlei Chen. Mobaiir: Unleashing sensor mobility for city-scale and fine-grained air-quality monitoring with airbert. In *Proceedings of the 22nd Annual International Conference on Mobile Systems, Applications and Services*, pages 223–236, 2024.
 - [58] Nan Zhou, Yuxuan Liu, Haoyang Wang, Fanhang Man, Jingao Xu, Fan Dang, Chaopeng Hong, Yunhao Liu, Xiao-Ping Zhang, Yali Song, et al. Catua: Catalyzing urban air quality intelligence through mobile crowd-sensing. *IEEE Transactions on Mobile Computing*, 2025.
 - [59] Zuxin Li, Fanhang Man, Xuecheng Chen, Susu Xu, Fan Dang, Xiao-Ping Zhang, and Xinlei Chen. Quest: Quality-informed multi-agent dispatching system for optimal mobile crowdsensing. In *IEEE INFOCOM 2024-IEEE Conference on Computer Communications*, pages 1811–1820. IEEE, 2024.
 - [60] Yunfan Wang, Steve Young, Demba Komma, Jaechan Lim, Zhen Feng, Zichen Fan, Chien-wei Tseng, Hun-Seok Kim, and David Blaauw. Global localization of energy-constrained miniature rf emitters using low earth orbit satellites. In *Proceedings of the 21st ACM SenSys*, pages 403–416, 2023.
 - [61] Huixin Dong, Yirong Xie, Xianan Zhang, Wei Wang, Xinyu Zhang, and Jianhua He. Gpsmirror: Expanding accurate gps positioning to shadowed and indoor regions with backscatter. In *Proceedings of the 29th ACM MobiCom*, pages 1–15, 2023.
 - [62] Jingao Xu, Hao Cao, Danyang Li, Kehong Huang, Chen Qian, Longfei Shangguan, and Zheng Yang. Edge assisted mobile semantic visual slam. In *Proceedings of the IEEE INFOCOM*, pages 1828–1837. IEEE, 2020.
 - [63] Haoyang Wang, Xuecheng Chen, Yuhao Cheng, Chenye Wu, Fan Dang, and Xinlei Chen. H-swarmloc: efficient scheduling for localization of heterogeneous mav swarm with deep reinforcement learning. In *Proceedings of the 20th ACM Conference on Embedded Networked Sensor Systems*, pages 1148–1154, 2022.
 - [64] Hongfei Xue, Qiming Cao, Yan Ju, Haochen Hu, Haoyu Wang, Aidong Zhang, and Lu Su. M4esh: mmwave-based 3d human mesh construction for multiple subjects. In *Proceedings of the 20th ACM SenSys*, pages 391–406, 2022.
 - [65] Yuze He, Li Ma, Jiahe Cui, Zhenyu Yan, Guoliang Xing, Sen Wang, Qintao Hu, and Chen Pan. Automatch: Leveraging traffic camera to improve perception and localization of autonomous vehicles. In *Proceedings of the 20th ACM SenSys*, pages 16–30, 2022.
 - [66] Jirong Zha, Yuxuan Fan, Xiao Yang, Chen Gao, and Xinlei Chen. How to enable llm with 3d capacity? a survey of spatial reasoning in llm. *arXiv preprint arXiv:2504.05786*, 2025.
 - [67] Ali J Ben Ali, Marziye Kouroshli, Sofiya Semenova, Zakieh Sadat Hashemifar, Steven Y Ko, and Karthik Dantu. Edge-slam: Edge-assisted visual simultaneous localization and mapping. *ACM Transactions on Embedded Computing Systems*, 22(1):1–31, 2022.
 - [68] Haoyang Wang, Jingao Xu, Chenyu Zhao, Zihong Lu, Yuhao Cheng, Xuecheng Chen, Xiao-Ping Zhang, Yunhao Liu, and Xinlei Chen. Transformloc: Transforming mavs into mobile localization infrastructures in heterogeneous swarms. *Proceedings of the IEEE INFOCOM*, 2024.
 - [69] Weichen Zhang, Ruiying Peng, Chen Gao, Jianjie Fang, Xin Zeng, Kaiyuan Li, Ziyu Wang, Jinqiang Cui, Xin Wang, Xinlei Chen, et al. The point, the vision and the text: Does point cloud boost spatial reasoning of large language models? *arXiv preprint arXiv:2504.04540*, 2025.
 - [70] Jiahe Cui, Shuyao Shi, Yuze He, Jianwei Niu, Guoliang Xing, and Zhenchao Ouyang. {VILAM}: Infrastructure-assisted 3d visual localization and mapping for autonomous driving. In *21st USENIX NSDI*, pages 1831–1845, 2024.
 - [71] Zhuozhu Jian, Qixuan Li, Shengtao Zheng, Xueqian Wang, and Xinlei Chen. Lvcp: Lidar-vision tightly coupled collaborative real-time relative positioning. *arXiv preprint arXiv:2407.10782*, 2024.
 - [72] Huajie Wu, Yihang Li, Wei Xu, Fanze Kong, and Fu Zhang. Moving event detection from lidar point streams. *nature communications*, 15(1):345, 2024.
 - [73] Xinlei Chen, Carlos Ruiz, Sihan Zeng, Liyao Gao, Aavek Purohit, Stefano Carpin, and Pei Zhang. H-drunkwalk: Collaborative and adaptive navigation for heterogeneous mav swarm. *ACM Transactions on Sensor Networks (TOSN)*, 16(2):1–27, 2020.
 - [74] Xinlei Chen, Aavek Purohit, Carlos Ruiz Dominguez, Stefano Carpin, and Pei Zhang. Drunkwalk: Collaborative and adaptive planning for navigation of micro-aerial sensor swarms. In *Proceedings of the 13th ACM SenSys*, pages 295–308, 2015.
 - [75] Xiaopeng Zhao, Guosheng Wang, Zhenlin An, Qingrui Pan, and Lei Yang. Understanding localization by a tailored gpt. In *Proceedings of the 22nd ACM MobiSys*, pages 318–330, 2024.
 - [76] Baining Zhao, Ziyu Wang, Jianjie Fang, Chen Gao, Fanhang Man, Jinqiang Cui, Xin Wang, Xinlei Chen, Yong Li, and Wenwu Zhu. Embodied-r: Collaborative framework for activating embodied spatial reasoning in foundation models via reinforcement learning. *arXiv preprint arXiv:2504.12680*, 2025.
 - [77] Chenyu Zhao, Ciyu Ruan, Jingao Xu, Haoyang Wang, Shengbo Wang, Jiaqi Li, Jirong Zha, Zheng Yang, Yunhao Liu, Xiao-Ping Zhang, et al. Foes or friends: Embracing ground effect for edge detection on

- lightweight drones. In *Proceedings of the 30th Annual International Conference on Mobile Computing and Networking*, pages 1377–1392, 2024.
- [78] Chenyu Zhao, Haoyang Wang, Jiaqi Li, Fanhang Man, Shilong Mu, Wenbo Ding, Xiao-Ping Zhang, and Xinlei Chen. Smoothlander: A quadrotor landing control system with smooth trajectory guarantee based on reinforcement learning. In *Proceedings of the 2023 ACM UbiComp*, pages 682–687, 2023.
- [79] Zhuozhu Jian, Zejia Liu, Haoyu Shao, Xueqian Wang, Xinlei Chen, and Bin Liang. Path generation for wheeled robots autonomous navigation on vegetated terrain. *IEEE Robotics and Automation Letters*, 2023.
- [80] Kyle Harlow, Hyesu Jang, Timothy D. Barfoot, Ayoung Kim, and Christoffer Heckman. A new wave in robotics: Survey on recent mmwave radar applications in robotics. *IEEE Transactions on Robotics*, 40:4544–4560, 2024.
- [81] A. Soumya, C. Krishna Mohan, and Linga Reddy Cenkeramaddi. Recent advances in mmwave-radar-based sensing, its applications, and machine learning techniques: A review. *Sensors*, 23(21), 2023.
- [82] Suhare Solaiman, Emad Alsuwat, and Rajwa Alharthi. Simultaneous tracking and recognizing drone targets with millimeter-wave radar and convolutional neural network. *Applied System Innovation*, 6(4), 2023.
- [83] Heba Abdelnasser, Mohammad Heggo, Oscar Pang, Mirko Kovac, and Julie A. McCann. Radro: Indoor drone tracking using millimeter wave radar. *Proc. ACM Interact. Mob. Wearable Ubiquitous Technol.*, 8(3), September 2024.
- [84] Yadong Li, Dongheng Zhang, Ruixu Geng, Zhi Lu, Zhi Wu, Yang Hu, Qibin Sun, and Yan Chen. A high-resolution handheld millimeter-wave imaging system with phase error estimation and compensation. *Communications Engineering*, 3, 2024.
- [85] Kai Zheng, Kun Qian, Timothy Woodford, and Xinyu Zhang. Neuroradar: A neuromorphic radar sensor for low-power iot systems. In *Proceedings of the 21st ACM Conference on Embedded Networked Sensor Systems*, pages 223–236, 2023.
- [86] Nader Al-Iqubaydhi, Abdulrahman Alenezi, Turki Alanazi, Abdulrahman Senyor, Naif Alanezi, Bandar Alotaibi, Munif Alotaibi, Abdul Razaque, and Salim Hariri. Deep learning for unmanned aerial vehicles detection: A review. *Computer Science Review*, 51:100614, 2024.
- [87] Simon Chadwick, Will Maddern, and Paul Newman. Distant vehicle detection using radar and vision. In *2019 International Conference on Robotics and Automation (ICRA)*, pages 8311–8317. IEEE, 2019.
- [88] Hyunggi Cho, Young-Woo Seo, BVK Vijaya Kumar, and Ragu-nathan Raj Rajkumar. A multi-sensor fusion system for moving object detection and tracking in urban driving environments. In *2014 IEEE international conference on robotics and automation (ICRA)*, pages 1836–1843. IEEE, 2014.
- [89] Danyang Li, Jingao Xu, Zheng Yang, Qian Zhang, Qiang Ma, Li Zhang, and Pengpeng Chen. Motion inspires notion: self-supervised visual-lidar fusion for environment depth estimation. In *Proceedings of the 20th ACM MobiSys*, pages 114–127, 2022.
- [90] Chenggao Li, Qianyi Huang, Yuxuan Zhou, Yandao Huang, Qingyong Hu, Huangxun Chen, and Qian Zhang. Riscan: Ris-aided multi-user indoor localization using cots wi-fi. In *Proceedings of the 21st ACM SenSys*, pages 445–458, 2023.
- [91] Weiguo Wang, Yuan He, Meng Jin, Yimiao Sun, and Xiuzhen Guo. Meta-speaker: Acoustic source projection by exploiting air nonlinearity. In *Proceedings of the 29th ACM MobiCom*, pages 1–15, 2023.
- [92] Hongfei Xue, Qiming Cao, Chenglin Miao, Yan Ju, Haochen Hu, Aidong Zhang, and Lu Su. Towards generalized mmwave-based human pose estimation through signal augmentation. In *Proceedings of the 29th ACM MobiCom*, pages 1–15, 2023.
- [93] Yuze He, Chen Bian, Jingfei Xia, Shuyao Shi, Zhenyu Yan, Qun Song, and Guoliang Xing. Vi-map: Infrastructure-assisted real-time hd mapping for autonomous driving. In *Proceedings of the 29th ACM MobiCom*, pages 1–15, 2023.
- [94] Shuyao Shi, Neiweng Ling, Zhehao Jiang, Xuan Huang, Yuze He, Xiaoguang Zhao, Bufang Yang, Chen Bian, Jingfei Xia, Zhenyu Yan, et al. Soar: Design and deployment of a smart roadside infrastructure system for autonomous driving. In *Proceedings of the 30th ACM MobiCom*, pages 139–154, 2024.
- [95] Jingao Xu, Guoxuan Chi, Zheng Yang, Danyang Li, Qian Zhang, Qiang Ma, and Xin Miao. Followupar: Enabling follow-up effects in mobile ar applications. In *Proceedings of the 19th ACM MobiSys*, pages 1–13, 2021.
- [96] Ali Safa, Tim Verbelen, Ilja Ocket, André Bourdoux, Hichem Sahli, Francky Catthoor, and Georges Gielen. Fusing event-based camera and radar for slam using spiking neural networks with continual stdp learning. In *2023 IEEE International Conference on Robotics and Automation (ICRA)*, pages 2782–2788. IEEE, 2023.
- [97] Rong Ding, Haiming Jin, Jianrong Ding, Xiaocheng Wang, Guiyun Fan, Fengyuan Zhu, Xiaohua Tian, and Linghe Kong. Push the limit of single-chip mmwave radar-based egomotion estimation with moving objects in fov. In *Proceedings of the 21st ACM SenSys*, pages 417–430, 2023.
- [98] Wenwei Li, Ruofeng Liu, Shuai Wang, Dongjiang Cao, and Wenchao Jiang. Egocentric human pose estimation using head-mounted mmwave radar. In *Proceedings of the 21st ACM SenSys*, pages 431–444, 2023.
- [99] Leon Müller, Manolis Sifalakis, Sherif Eissa, Amirreza Yousefzadeh, Paul Detterer, Sander Stuijk, and Federico Corradi. Aircraft marshaling signals dataset of fmcw radar and event-based camera for sensor fusion. In *2023 IEEE Radar Conference (RadarConf23)*, pages 01–06. IEEE, 2023.
- [100] Yanxiang Wang, Yiran Shen, Kenuo Xu, Mahbub Hassan, Guangrong Zhao, Chenren Xu, and Wen Hu. Towards high-speed passive visible light communication with event cameras and digital micro-mirrors. In *Proceedings of the 22nd ACM Conference on Embedded Networked Sensor Systems*, pages 704–717, 2024.